Dynamic Approach to Behavior-Based Robotics

Design, Specification, Analysis, Simulation and Implementation

Dissertation submitted by
Estela Bicho
to the University of Minho
for the Degree of Doctor on Industrial Electronics
in the Branch of Automation and Control

Guimarães, Portugal

September, 1999

Contents

Chapter 4

Using attractor dynamics to control motion based on low-level distance sensors

This chapter demonstrates (see also Bicho, Mallet and Schöner, 1999b) that the dynamic approach to path planning (Schöner and Dose, 1992) lends itself naturally to implementation on simple autonomous vehicles using only low-level sensory information such as distances sensed by infra-red detectors or sonars. It also shows how theoretical design and hardware implementation are enchained effortlessly. The chapter starts with a review of the literature in the domain of path planning so that we can position the dynamic approach to path planning with respect to the other approaches. Section 4.2 presents a dynamical system that generates a time series of the vehicle's heading direction. Each sensor is assumed to contribute a repulsive force-let to the vector-field of this dynamical system and their sum leads to obstacle avoidance. Movement toward the target is achieved by adding an attractive force-let. Next, Section 4.3 explains how the vehicle's path velocity can be controlled such that the system is near an attractor at all times. Section 4.4 presents some implementation details. Experimental results that demonstrate the properties of the path generating system and the velocity control system are presented in Section 4.5. Finally, the chapter ends with conclusions.

4.1 Introduction

Motion planning is an essential part of an autonomous robot system (Latombe, 1991). In the basic variation of motion planning for a mobile robot, the task is to generate a collision-free vehicle path that brings the robot system to a specified target location. The majority of the research in this domain has been conducted, in the field of robotics, under the title of path planning. Even-though motion planning has been studied for two decades and a large body of research reported in the

literature exists, the design of a simple and reliable path generating (planning and motion control) system is still a challenge.

The problem has been addressed in theoretical work by isolating the path planning aspect from the aspects of obtaining sensory information about the world and controlling vehicle motion to generate the path (review, e.g., in Latombe, 1991; chapters 4 and 7 in Cox, Wilfong, 1990; Kortenkamp, 1998; Pruski, 1998).

Classical theoretical approaches to the problem, also called model-based planning, assume that complete knowledge of the world's geometry is known prior to the planning stage (Lozano-Perez and Wesley, 1979; Schwartz and Sharir, 1983; Cameron, 1998). The objective is to find a connected sequence of collision-free spaces for a finite-size object (a robot), from an initial position to a target position, typically based on polygonal representations of the objects in the world. Some of these theoretical approaches propose algorithms that guarantee that kinematic and dynamic constraints are fulfilled and that a path is found if one exists (Gilbert and Jonhson, 1985; Shin and Mckay, 1985; Kim and Shin, 1985; Kedem and Sharir, 1988). A path is then generated by piecing together the free spaces or by tracing around the forbidden areas (Brooks, 1983; Singh and Wagh, 1987; Takahashi and Schilling, 1989) .

After the planning stage, the robot has to control its motion along the nominal path. The major difficulty here is due to the uncertainties because of unprecise world modeling and/or changes in the robot environment, e.g. appearance and disappearance of objects, and moving objects (Laumond, 1993; Hu and Brady, 1997). First, the path has been computed from unprecise geometric models of the environment. Either the planned path is guaranteed to be safe with respect to these uncertainties, or the robot has to check its safety in the real world. Second, the robot does not perfectly execute the nominal path. Motion planning in the presence of uncertainties and feedback control gave rise to the necessity of sensor based motion planning (Feng and Krogh, 1990). However, it is not possible to simply add a step to acquire sensory information, and then rebuilt the world model and re-plan a collision free path dynamically using these classical schemes (i.e. computational geometry methods) since they are very difficult to obtain and maintain in real time. This also poses the problem of the overall control-theoretic stability of the path generation systems, as the step-wise computation of representations of obstacles and targets is not characterized by a time scale. Thus it might be difficult to satisfy Brockett's necessary condition of systems controllable by smooth feedback (Brockett, 1983).

In contrast to the approaches described above, the potential field approach uses a scalar function to describe both objects and free space (Khatib, 1986). The target location is modeled with an attractive potential and the obstacles with repulsive potentials. Traditional potential field methods typically consider all obstacles at every point in the world. The path is then generated by following the negative gradient of the overall potential function. Although this approach can be computationally efficient (Barraquand and Latombe, 1991) and is suitable for on-line feedback

control (Feng and Krogh, 1992) it suffers from local minima, which may cause the path to terminate at a point other than the target location. Some solutions have been proposed that attempt to overcome this limitation (Cannolly, Burns and Weiss, 1990; Rimon and Koditschek, 1992).

The above approaches rely upon global representations of the world in which the robot operates. Another approach to the navigation problem is to define instead a local representation of the space around the robot (e.g. Lumelsky and Stepanov, 1986; Lumelsky and Stepanov, 1987). Still another possibility is the limit case where sensory information is used at low levels of parameter extraction which is not typically represented (Brooks, 1986; Borenstein and Koren, 1989; Zapata, Lepinay and Thompson, 1994; Fujimori, Nikiforuk and Gupta, 1997). This later approach is usually called sensor-based motion planning.

Among all the approaches, the potential field approach is one of the most popular to date. The main reason is that this approach is suitable for on-line feedback control (Arkin, 1989; Arkin, 1998).

The dynamic approach to path planning and control (Schöner and Dose, 1992) makes this linkage to control even stronger by replacing the transient solutions of the potential field approach with attractor solutions (asymptotically stable states) of a dynamical system, that therefore contributes to the asymptotically stability of the overall control scheme.

In the planning dynamics, that is, in the equations of motion, the vector field is specified so that it captures the task constraints as component forces that define attractors or repellers of the dynamical system. An attractive force serves to attract the system to the direction at which the target lies, and repulsive forces are used to avoid the directions at which obstacles are located. Since some of these forces have limited range from their superposition a non-linear dynamical system results. By design the system is tuned so that the planning variable is in a resulting attractor of this dynamics most of the time. Thus, the path is in fact generated by an attractor solution and not by a transient solution of the dynamical system.

This way one can avoid the difficult problem of designing a non-linear dynamical system all transient solutions of which fulfill multiple constraints. By contrast, designing a dynamical system, the attractors of which fulfill particular constraints, is possible by making use of the qualitative theory of dynamical systems (Perko, 1991). Qualitative changes in the robot's behavior arise through changes in the number, nature, and stability of fixed points. Such changes correspond to bifurcations in the vector field. Local bifurcation theory helps to make design decisions around points, at which the system must switch from one type of solution to another (Schöner, Dose and Engels, 1995). The values of model parameters can be chosen in part based on such analyses.

4.2 The attractor dynamics of heading direction

The dynamic approach to path generation in autonomous vehicles (Schöner and Dose, 1992; Schöner, Dose and Engels, 1995) employs the heading direction, ϕ, relative to some external world axis as the planning variable. The path plan is a time course of this variable which is obtained in time as attractor solutions of a dynamical system for the heading direction.

Task constraints are component forces which are cast together into the vector field of this dynamical system. For example, the directions $\phi = \psi_{obs}$ (relative to a fixed external world axis) in which obstacles lie from the view point of the robot, and similarly, the direction $\phi = \psi_{tar}$ in which the target lies are constraints that are represented by repulsive and attractive force-lets acting on the heading direction (see Figure 4.1). In isolation, each force-let erects an attractor (asymptotically stable state) or a repeller (unstable state) of the dynamics of the planning variable, ϕ. The attractive force-let serves to attract the system to the desired value of the heading direction (here the direction in which the target lies). A repulsive force-let is used to avoid that the system takes an undesired value (here the direction in which an obstacle lies). By design, the system is operated so that the heading direction is in or near a resulting attractor of this dynamics. As the vehicle moves, the directions to the obstacles and target in the world changes, so that the resulting attractor shifts, pulling the heading direction along (Figure 4.2).

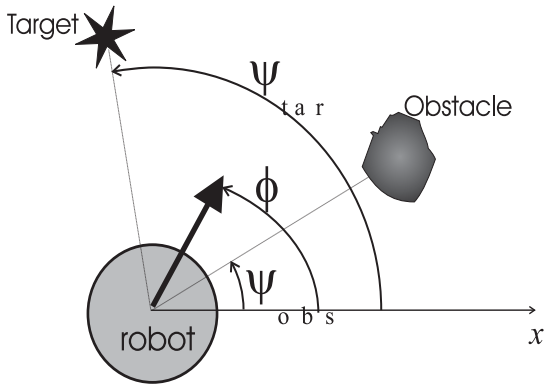

Figure 4.1: Constraints for the dynamics of ϕ are the directions at which obstacles and target lie from the current position of the robot, i.e. directions ψ_{obs} and ψ_{tar}.

Because all angles are measured in an external reference frame, the contributions of the obstacles′ and the target to the dynamical system of heading direction do not depend on the current orientation of the robot.

In Schöner and Dose (1992) and Schöner, Dose and Engels (1995) representations of the locations of obstacles in the external reference frame were obtained from a computer vision system, that employed the method of inverse perspective projection (Mallot, Bültoff, Little and Bohrer, 1991) based on a cali-

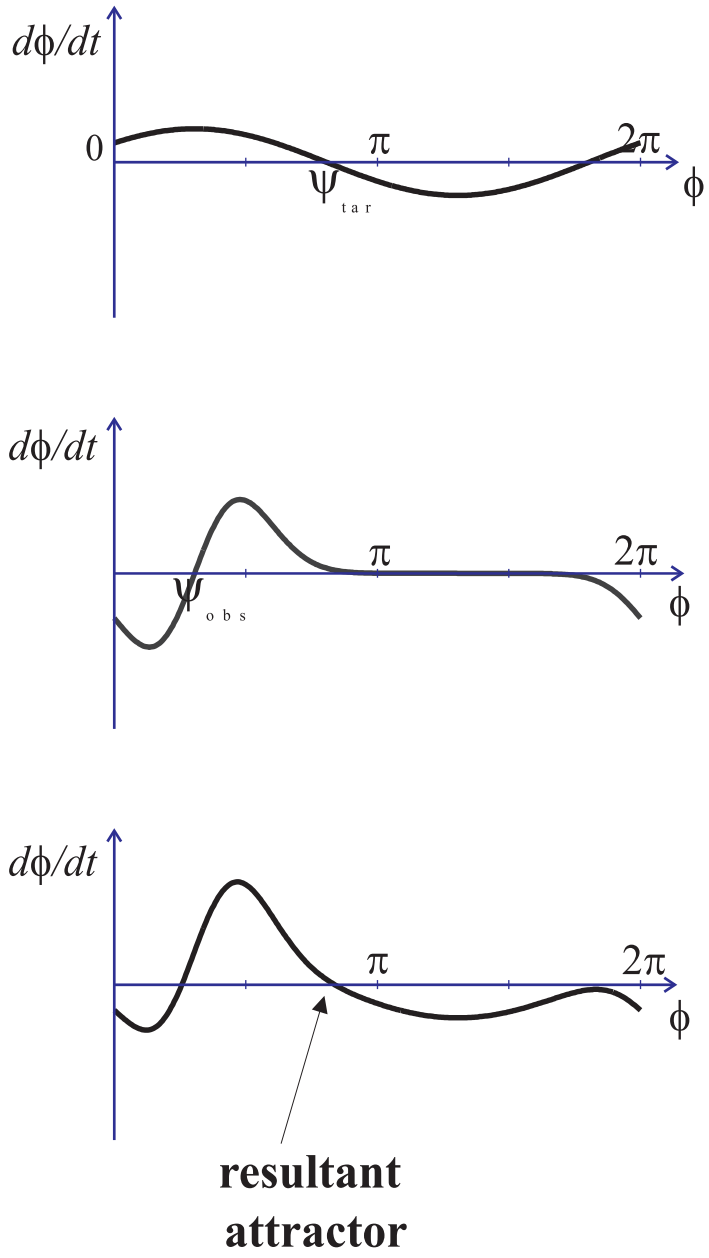

Figure 4.2: Resultant attractor (bottom Panel) from the superposition of the repulsive force-let (middle Panel) from obstacle constraints and attractive force (top Panel) due to the target constraint. Parameters must be tuned so that the system is relaxed in the attractor.

brated camera geometry. Thus, if the robot was rotated on the spot, the directions to the objects in the world did not change and thus the dynamics of heading direction was independent of the current value of heading direction. Only because this

was true did the resultant dynamics have attractors and repellers as designed.

The question we address here is how can this approach be applied to our lower level vehicles, which know nothing about external reference frames, nothing about objects resting in the world, but have only their own low-level sensory information to generate a dynamics of heading direction? We answer this question in the next subsection.

4.2.1 Obstacle avoidance

The vehicle used in this project has seven infra-red sensors mounted on a ring which is centered on the robot's rotation axis. These infra-red sensors are used to measure the distance to surfaces at the height of the ring (see Section 3.2).

On this low-level platform, each distance sensor points into a fixed direction, θ_i, in a reference frame fixed to the robot body. Thus each distance sensor looks into a direction, $\psi_i = \phi + \theta_i$, in an external reference frame if ϕ is the heading direction in such an external frame. This is illustrated in Figure 4.3.

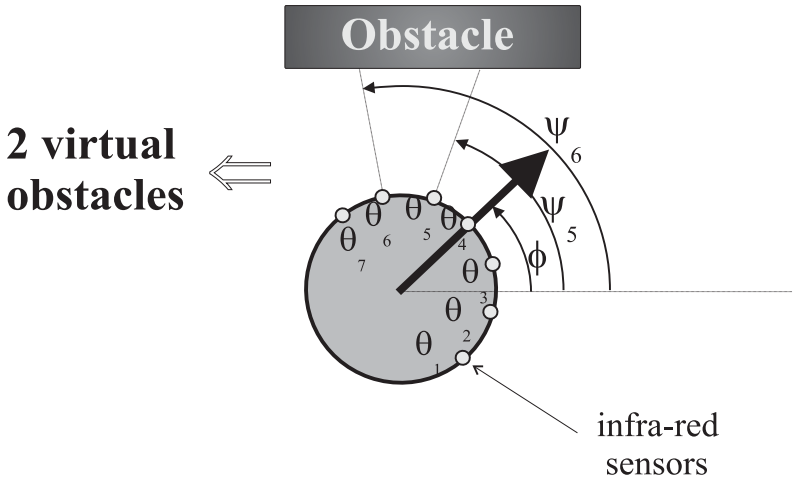

Figure 4.3: Each sensor i ($i = 1, \ldots, 7$), which is mounted at angle θ_i relative to the frontal direction, specifies an obstacle at direction $\psi_i = \phi + \theta_i$ in an external reference frame. In the figure, sensors 5 and 6 specify virtual obstacles at ψ_5 and ψ_6 respectively.

Our strategy is now simply to say that each sensor i ($i = 1, 2, \ldots, 7$) specifies a virtual obstacle in that direction ψ_i, if an obstruction is detected there, so that repulsive force-lets centered at these directions are erected. Each repulsive force-let reads (see Figure 4.4):

$$f_{\text{obs},i}(\phi) = \lambda_i(\phi - \psi_i) \exp\left[\frac{-(\phi - \psi_i)^2}{2\sigma_i^2}\right] \quad i = 1, 2, \ldots, 7 \tag{4.1}$$

In this equation only the difference $\phi - \psi_i = -\theta_i$, which is fixed and known,

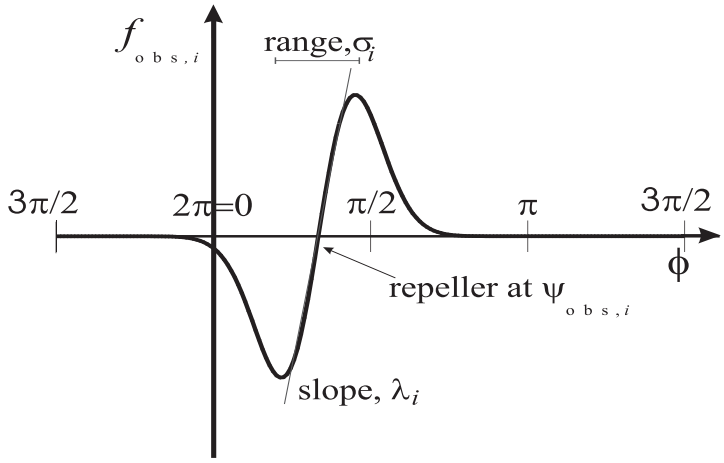

Figure 4.4: A contribution to the dynamics of heading direction expressing the task constraint "avoid moving toward obstacles" is a force-let with a zero-crossing at the direction, $\psi_{\text{obs},i}$ at which an obstruction has been detected. Every distance sensor ($i = 1, 2, \ldots, 7$) contributes such a force-let centered on the direction in which the sensor points. The positive slope of force at the zero-crossing makes that direction a repeller. By decreasing this slope with increasing measured distance, only nearby surfaces repel strongly. The range of the force-let is limited based on sensor range and on the constraint of passing without contact.

enters into the dynamics of the heading direction. This renders the performance independent from the calibration of the planning coordinate system. The strength of repulsion, $\lambda_i > 0$, from the virtual obstacle at direction ψ_i, is a decreasing function of the sensed distance, d_i:

$$\lambda_i = \beta_1 \exp\left[-\frac{d_i}{\beta_2}\right] \tag{4.2}$$

where β_1 controls the maximum repulsion strength of this contribution, and β_2 controls the rate of decay with increasing distance. Thus, when no surface is within the range of the distance sensor, then the corresponding force-let is zero and drops out of the dynamics of heading direction.

The angular range over which the force-let exerts its repulsive effect is determined by σ_i, which depends on the sensor sector, $\Delta\theta$ (= 30 deg), and also on the distance, d_i, because the angle subentended by half the vehicle at the sensed distance is added on each side of the sensor sector as a safety margin:

$$\sigma_i = \arctan\left[\tan\left(\frac{\Delta\theta}{2}\right) + \frac{R_{\text{robot}}}{R_{\text{robot}} + d_i}\right] \tag{4.3}$$

The first term reflects the angular range, $\Delta\theta$, over which the infra-red sensor may detect reflected light, while the second term expresses the additional angle required for the robot to pass next to an obstacle that would occupy maximally the entire sensor range. The further away the robot is from the obstacle, the smaller the angular safety margin, because the angle subentended by the robot itself when next to the obstacle decreases as is indicated. This is depicted in Figure 4.5.

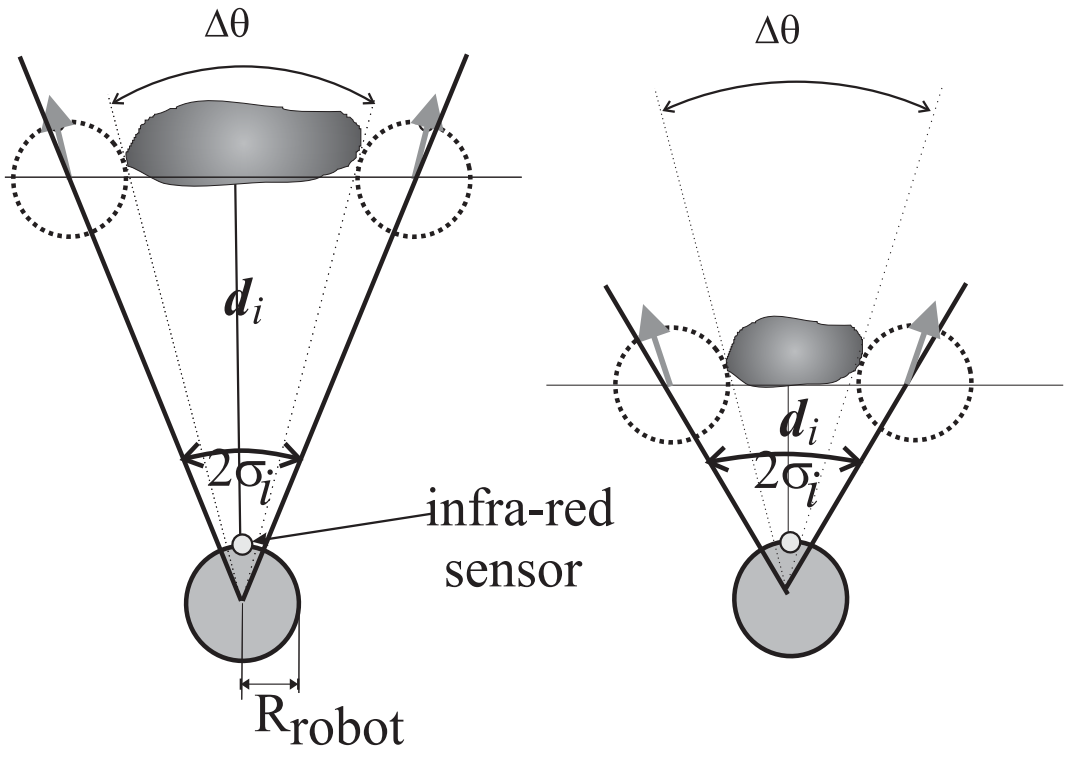

Figure 4.5: The range of the repulsive force-let is limited based on the sensor range and on the constraint of passing next to the virtual obstacle without contact.

The contributions from all the sensors are summed. Therefore, the overall obstacle avoidance dynamics reads:

$$\frac{d\phi}{dt} = F_{\text{obs}}(\phi) = \sum_{i=1}^{7} f_{\text{obs},i}(\phi) \tag{4.4}$$

Figures 4.6 and 4.7 illustrate that the summed obstacle contributions depend little on the current orientation of the vehicle.

In the situation depicted in Figure 4.3 two sensors respond to the obstacle. The sum of their contributions leads to a single repeller that covers the entire angular range subentended by the obstacle (see Figure 4.6). Figure 4.7 shows how at a different orientation of the sensors relative to the obstacle three sensors detect now

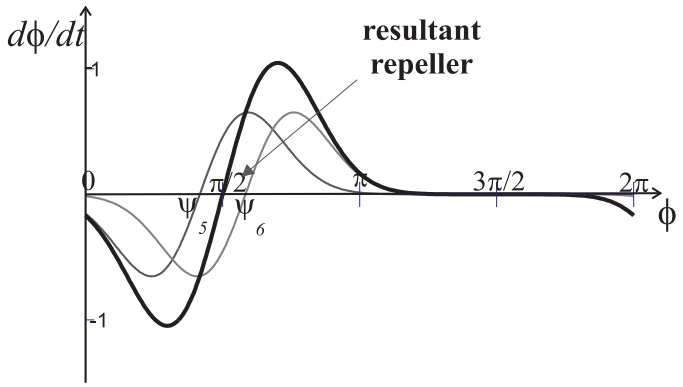

Figure 4.6: In the situation depicted in Figure 4.3 two virtual obstacles are detected, at directions ψ_5 and ψ_6. In that figure $\phi = \pi/4$ rad, $\psi_5 = 5\pi/12$ rad and $\psi_6 = 7\pi/12$ rad, the sensed distances are both 35 cm. Two repulsive force-lets centered at these directions are therefore erected (solid thin lines). The solid bold line shows the resultant obstacle dynamics. The resultant repeller is at $\pi/2$ rad.

the obstacle, leading to changed individual repulsive force-lets. However, their sum erects a repeller at approximately the same direction with respect to the external reference frame. This result thus shows that the dynamics for the heading direction has indeed the designed structure with the repellers and attractors at the right location, as it is invariant under rotations of the vehicle on the spot. This invariance is, of course, constrained by the number of sensors disposed around the robot. The more sensors are used the more invariant the dynamics is.

4.2.2 Target acquisition

As a simple variation of the "find-goal problem" we assume that the absolute coordinates of the target are known. A second, more higher level, variation of this problem is to leave for the robot the responsibility of determining the target location based on its own sensory information (see Chapter 6 and Bicho, Mallet and Schöner, 1999a).

For simplicity, because in this chapter we want to focus on the problem of path planning and motion control, the target is given in external coordinates (X_{target},Y_{target}). The robot keeps an estimate of its own location, ($X_{\text{robot}}, Y_{\text{robot}}$), in the external reference frame by integrating motor commands, through the dead-reckoning mechanism, from an initial reference position:

$$\frac{dX_{\text{robot}}}{dt} = v\cos(\phi) \tag{4.5}$$

$$\frac{dY_{\text{robot}}}{dt} = v\sin(\phi) \tag{4.6}$$

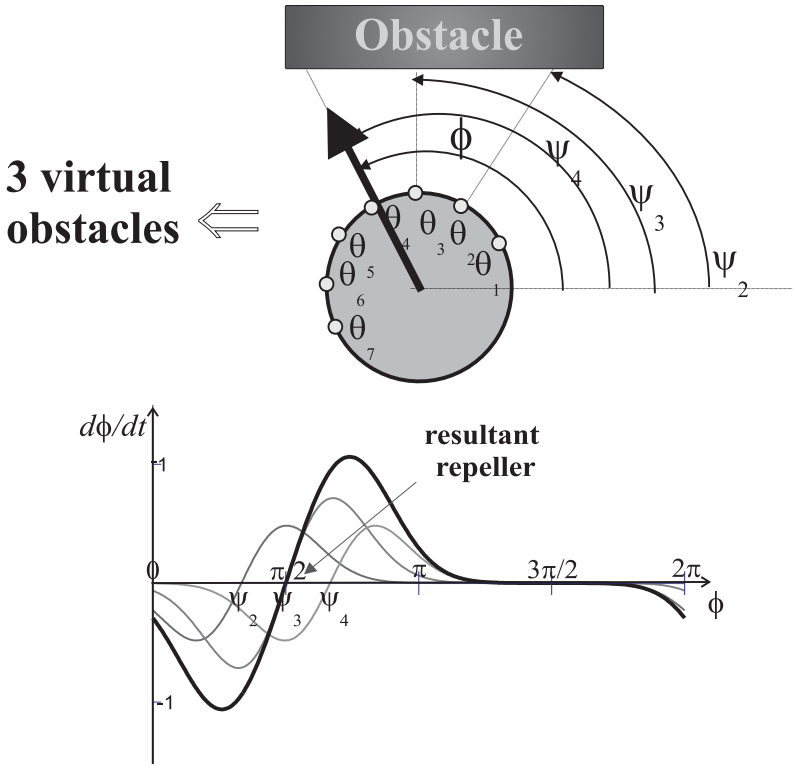

Figure 4.7: On the top: with respect to Figure 4.6 the robot turned left $5\pi/12$ rad. From this rotation three virtual obstacles at directions ψ_2, ψ_3 and ψ_4 result. In this figure $\phi = 2\pi/3$ rad, $\psi_2 = \pi/3$ rad, $\psi_3 = \pi/2$ rad and $\psi_4 = 2\pi/3$ rad. Distances are 40, 30 and 40 cm respectively. On the bottom: three repulsive force-lets are erected at these directions. The bold line represents the resultant obstacle avoidance dynamics. The resultant repeller is near $\pi/2$.

Where v is the path velocity and ϕ the heading direction as obtained from the planning dynamics. The direction, ψ_{tar}, relative to the x-axis, in which the target lies as "seen" from the current position of the robot is:

$$\psi_{\text{tar}} = \arctan\left(\frac{Y_{\text{target}} - Y_{\text{robot}}}{X_{\text{target}} - X_{\text{robot}}}\right) \tag{4.7}$$

The orientation toward the target, is specified by erecting an attractor at direction ψ_{tar} with strength λ_{tar}. Because target acquisition is desired from any starting orientation of the robot the range over which this contribution exhibits its attractive effect, over the heading direction of the robot, ϕ, is the entire full circle (i.e. from 0 to 2π rad). The simplest mathematical form for this attractive force-let is (see Figure 4.8)

$$\frac{d\phi}{dt} = f_{\text{tar}}(\phi) = -\lambda_{\text{tar}} \sin(\phi - \psi_{\text{tar}}) \tag{4.8}$$

For this module the calibration of the dynamic variable heading direction, ϕ, does matter.

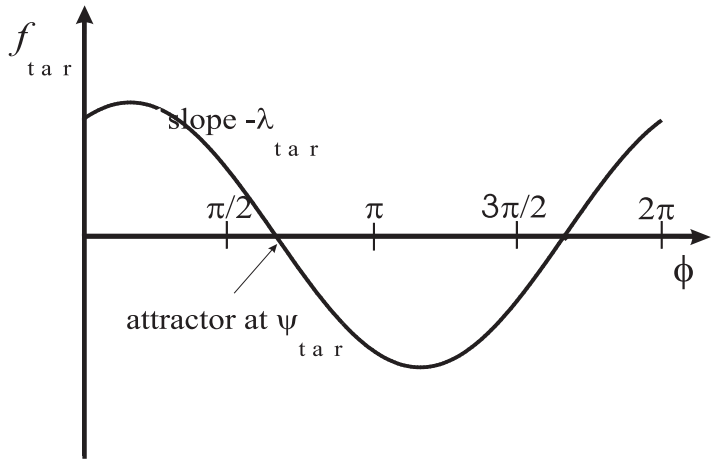

Figure 4.8: A contribution to the dynamics of heading direction expressing the task constraint "move toward targets" is a force with a zero-crossing at the specified direction toward the target, ψ_{tar}. The negative slope at the zero-crossing makes this an attractor of the dynamics. The target contribution is sinusoidal and extends over the entire range of heading direction. This leads to a repeller in the direction $\pi + \psi_{\text{tar}}$ opposite to ψ_{tar}.

4.2.3 Integrating the two behaviors

The integration of these two behaviors is obtained by summing obstacle and target contributions to the vector field:

$$\frac{d\phi}{dt} = F_{\text{obs}}(\phi) + f_{\text{tar}}(\phi) \tag{4.9}$$

Precedence of obstacle avoidance is accomplished making the strength of the obstacle contributions stronger than the target contribution. More sophisticated control over activation and deactivation of such contributions can be obtained using activation networks (see Steinhage and Schöner, 1997; Steinhage, 1998; Large, Christensen, Baczy, 1999) but is unnecessary here.

Figure 4.9 illustrates the simultaneous effect of target and obstacle constraints. In the depicted situation, the space between the two obstacles is not sufficient for the robot to pass between them. The target lies behind this opening, the most challenging situation for obstacle avoidance. The obstacle avoidance contribution

to the dynamics (solid thin line) generates a repeller at the direction in between the two obstacles, while the target contribution (dashed line) erects an attractor at this direction. The resultant dynamics (solid bold line) has a repeller at this direction because the obstacle contributions dominate.

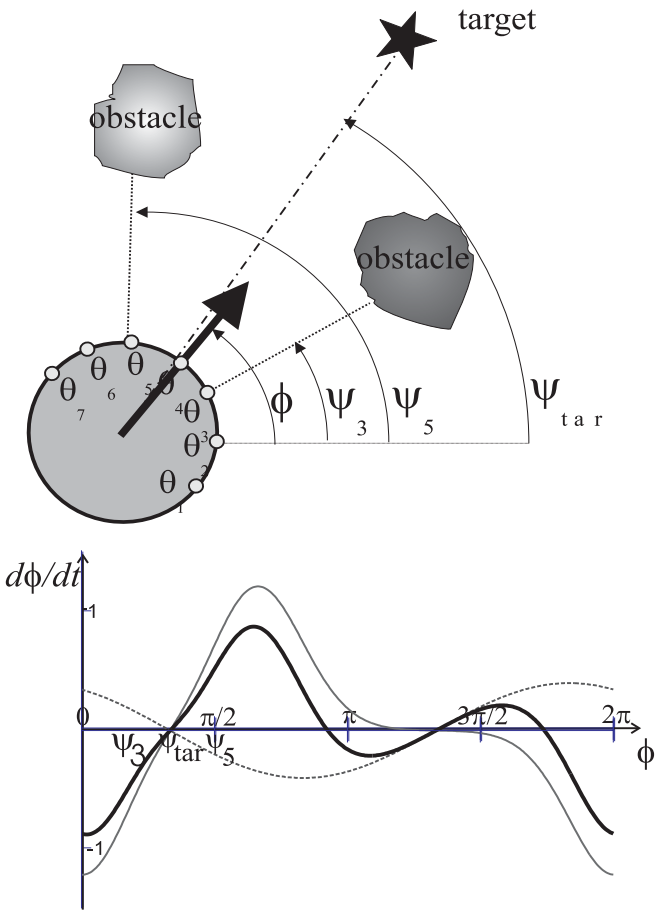

Figure 4.9: On the top: The distance between the obstacles is not sufficient for the robot to pass through, and the target lies in the direction pointing in between the two obstacles thus defying the obstacle avoidance behavior. On the bottom: Obstacle and target contributions for the dynamics are represented by the solid thin line and the dashed line respectively. The resulting dynamics is the solid bold line.

Qualitative changes of behavior arise if the number and stability of fixed points of the heading direction dynamics changes. These changes correspond to bifurcations of the vector field brought about by changing sensory information as the robot moves. For instance, an attractor pointing along a path leading between two obstacles may become unstable and turn into a repeller as the vehicle approaches the obstacles, and the obstacle contributions widen in angular range. At such bifurcations, the heading direction may come to lie exactly on a repeller (a former attractor that

turned unstable). To ensure escape from repellers within a limited time, the planning dynamics is augmented by a stochastic force

$$f_{\text{stoch}} = \sqrt{\mathcal{Q}}\xi_{\text{n}} \tag{4.10}$$

chosen as Gaussian white noise, ξ_{n}, of unit variance, so that $\mathcal{Q}$ is the effective variance of the force. This stochastic force is in addition to sensory and motor noise, which may vary as a function of environmental conditions. Since behaviors are generated by asymptotically stable states (attractors) the system is robust against noise.

The complete heading direction dynamics is therefore:

$$\frac{d\phi}{dt} = F_{\text{obs}}(\phi) + f_{\text{tar}}(\phi) + f_{\text{stoch}} \tag{4.11}$$

Planning decisions, i.e. qualitative changes in the behavior, arise through bifurcations in the vector field which are brought about as the vehicle moves or the environment changes.

4.3 Control of driving speed

As the robot moves sensory information changes and thus attractors (and repellers) shift. The same happens if obstacles move in the world. To keep the system stable, i.e. in or near an attractor at all times, the rate of such shifts must be limited to permit the system to track the attractor as it shifts. One way this can be accomplished is by controlling the path velocity, v, of the vehicle. This is because, the velocity with which the fixed points shift is determined by the relative velocity of the robot with respect to its environment. Let us analyze the rate of such shifts for the simplest case of the robot moving in a resting environment with constant velocity and heading direction. Figure 4.10 shows that for this case the maximal rate of change of obstacle or target bearing occurs when the corresponding objects are seen sideways.

We derive the relationship between the maximal rate of change, $\dot{\psi}_{\text{max}}$, and the vehicle's path velocity, v (see Figure 4.11): Let us assume that initially, $t = 0$ sec, the object (target or obstacle) is located exactly at a right angle to the current heading direction and at a distance d from the robot. At this instant in time the direction at which the object lies as seen from the current position of the vehicle and with respect to the external reference axis is $\psi_0 = 0$ rad. Δt later the vehicle has traveled a distance of $\Delta d_{\text{robot}} (= v\Delta t)$. Thus the object direction as seen from the new position of the robot is now

$$\psi_{\Delta\text{t}} = \arctan\left(\frac{\Delta d_{\text{robot}}}{d}\right) \tag{4.12}$$

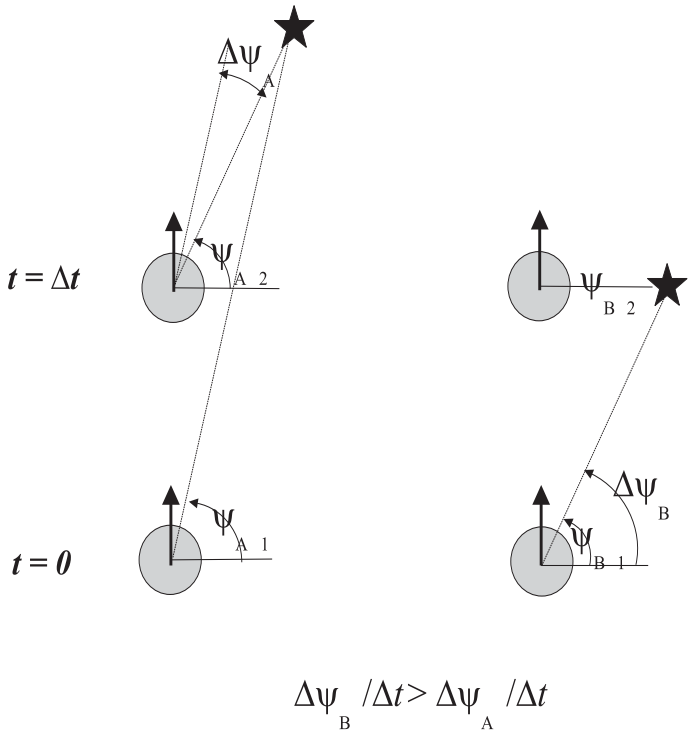

Figure 4.10: Rate of change of obstacle or target bearing (here represented by the black star) as the robot moves in a resting environment with constant movement direction. On the left: The obstacle or target lies far ahead. Initially, the robot is at the position indicated by $t = 0$. The direction at which the object is "seen" is ψ_{A1}. Later on the robot is at the position indicated by $t = \Delta t$. From this position the object is "seen" at direction ψ_{A2}. Thus, in the time interval Δt the rate of change of the object bearing is $\Delta\psi_{\mathrm{A}}/\Delta t$. On the right: The obstacle or target is "seen" sideways. In the same interval of time the rate of change of the object bearing is $\Delta\psi_{\mathrm{B}}/\Delta t$ and is larger than in the previous case.

For small $\Delta d_{\mathrm{robot}}/d$ we can write:

$$\psi_{\Delta \mathrm{t}} \approx \frac{\psi_0 - \psi_{\Delta \mathrm{t}}}{\Delta t} \approx \frac{v \Delta t}{d} \tag{4.13}$$

Therefore we can derive the maximal rate of shift of the fixed points as a function of the vehicle's velocity

$$\dot{\psi}_{\max} \approx \frac{\Delta \psi}{\Delta t} \approx \frac{v}{d} \tag{4.14}$$

This approximate description can be turn around to compute the desired path velocity as a function of distance with $\dot{\psi}_{\max}$ as a design parameter, that can be tuned

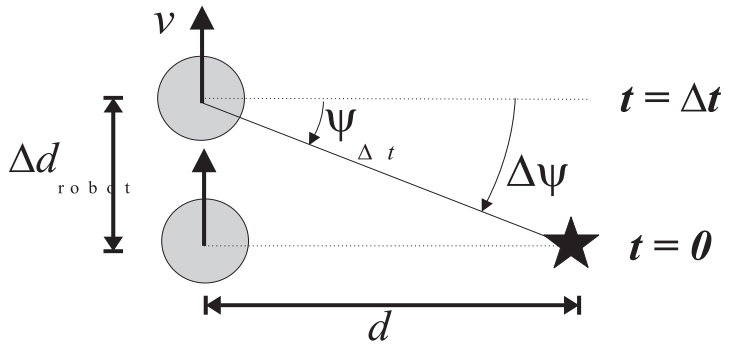

Figure 4.11: This figure illustrates the relationship between the maximal rate of change of obstacle or target bearing and the vehicle's path velocity, which occurs when the objects are seen sideways.

to obtain good tracking. We compute the desired velocity separately for each of the two constraints (i = tar or obs):

$$V_i = d_i \dot{\psi}_{\max} \tag{4.15}$$

The desired velocities are imposed through a very simple dynamics (Bicho, Schöner, 1997)

$$\begin{aligned} \frac{dv}{dt} = &-c_{\text{obs}} \left(v - V_{\text{obs}}\right) \exp\left[-\frac{(v - V_{\text{obs}})^2}{2\sigma_{\text{v}}^2}\right] \\ &-c_{\text{tar}} \left(v - V_{\text{tar}}\right) \exp\left[-\frac{(v - V_{\text{tar}})^2}{2\sigma_{\text{v}}^2}\right] \end{aligned} \tag{4.16}$$

The strengths, c_{obs} and c_{tar}, are adjusted such that in the presence of strong obstacle contributions the obstacle term dominates while in the absence of such contributions the reverse holds. A systematic way to construct a function that indicates if obstacle contributions are present, is to integrate the obstacle force-lets, from which a potential function of the obstacle avoidance dynamics results:

$$U(\phi) = \sum_{i=1}^{7} \left(\lambda_i \sigma_i^2 \exp\left[-\frac{(\phi - \psi_i)^2}{2\sigma_i^2}\right] - \lambda_i \sigma_i^2 / \sqrt{e} \right) \tag{4.17}$$

Positive values of this potential function indicate that the heading direction is in a repulsion zone of sufficient strength, λ_i, so $c_{obs} > 0$ and $c_{tar} = 0$ is required. Conversely, negative values of the potential indicate that the heading direction is outside the repulsion range or repulsion is weak, so now $c_{obs} = 0$ and $c_{tar} > 0$ is

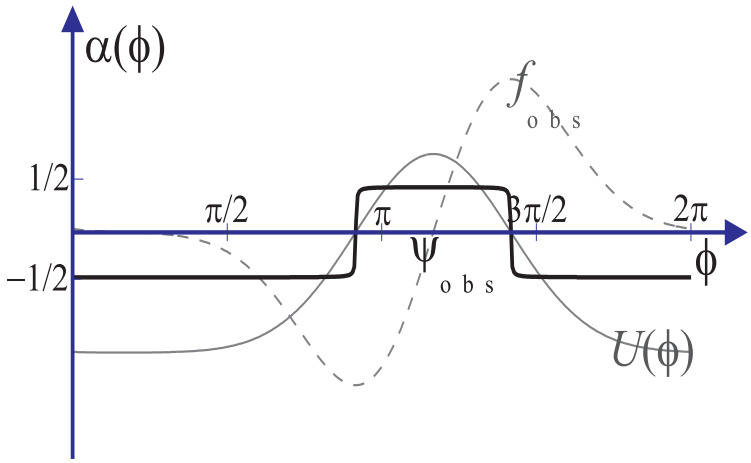

Figure 4.12: The dashed line is a repulsive force-let, f_{obs}. Its integral provides a potential (solid thin line), U, which is maximal near the heading direction to be avoided, i.e the resultant repeller. The thresholded potential (solid bold line), α, serves as an indicator function of those intervals of the heading direction from which obstacle forces repel.

required. The transformation of levels of the potential to the strengths of the two contributions to the velocity control makes use of a sigmoidal threshold function,

$$\alpha(\phi) = \arctan[cU(\phi)]/\pi \tag{4.18}$$

ranging from $-1/2$ to $1/2$ (see Figure 4.12). Finally we can write the following functions for the strengths of the two velocity contributions:

$$c_{\text{obs}} = c_{v,\text{obs}}\,(1/2 + \alpha\,(\phi)) \tag{4.19}$$

$$c_{\text{tar}} = c_{v,\text{tar}}\,(1/2 - \alpha\,(\phi)) \tag{4.20}$$

At sufficiently sharp sigmoids (c sufficiently large) this leads to the required transition behavior. The parameters, $c_{v,\text{tar}}$ and $c_{v,\text{obs}}$, determine the relaxation rate of the velocity dynamics in the two cases when either the obstacle or the target constraints dominate.

The following hierarchy of relaxation rates ensures that the system relaxes to the attractors and that obstacle avoidance has precedence over the target contribution:

$$\lambda_{\text{tar}} \ll c_{v,\text{tar}}, \quad \lambda_{\text{obs}} \ll c_{v,\text{obs}}, \quad \lambda_{\text{tar}} \ll \lambda_{\text{obs}} \tag{4.21}$$

4.4 Implementation on Robodyn

The complete dynamic architecture was implemented and tested on the mobile platform Robodyn.

In the implementation, the dynamics of heading direction, path velocity and the dead-reckoning equations are integrated numerically using the Euler method.

Sensory information is acquired once per computation cycle. The cycle time is measured and is approximately 50 ms. As the time step must be smaller than the fastest relaxation time on the system, this imposes minimal time scales on the entire dynamical architecture. Thus the computational cycle time is the limiting factor for determining the relaxation times of the dynamics in real time units and thus for the overall speed at which the robot's behavior evolves.

The rate of change of heading direction obtained from the dynamics of heading direction (Equation 4.11) directly specifies the angular velocity, w, of the robot for rotation around its center. This can be translated into the difference between left and right wheel rotation speed. The path velocity, v, specifies the average rotation speed of both wheels. Together, the rotation speeds of both wheels can be computed and are sent as set point to the velocity servos of the two motors (see Section 3.3).

4.5 Experimental results

We first discuss a number of results demonstrating the properties of the path planning system, then the velocity control system, and finally we present some sample trajectories of the vehicle in different scenarios.

4.5.1 Properties of the path planning dynamics

Decision making through bifurcations

The capability of the path planning system to make decisions is depicted in Figure 4.13, and discussed in more detail now. In the top Panel the robot faces two obstacles that are sufficiently far apart to pass in between. In this case the corresponding obstacle contributions to the vector field share little overlap. The resulting obstacle avoidance dynamics has repellers corresponding separately to each obstruction, and an attractor in between, which attracts the robot to pass between the obstacles. The target contribution also erects an attractor at the direction pointing in between the two obstacles. Obstacle and target contributions "cooperate" and give rise to a vector field with a strong attractor at that direction. Behaviorally this means that the behavior corresponding to proceed straight to the target becomes more stable, or put in another way, the decision to pass through the obstacles is reinforced. In the bottom Panel, the robot faces again two obstacles but this time they are positioned too close together for the robot to pass in between them. In the illustrated situation four obstructions (i.e. four virtual obstacles) are detected: two corresponding to the left obstacle while the other two to the right obstacle. The repulsive force-lets from these four virtual obstacles are sufficiently overlapping. Their superposition corresponds, therefore, to averaging among the repulsive

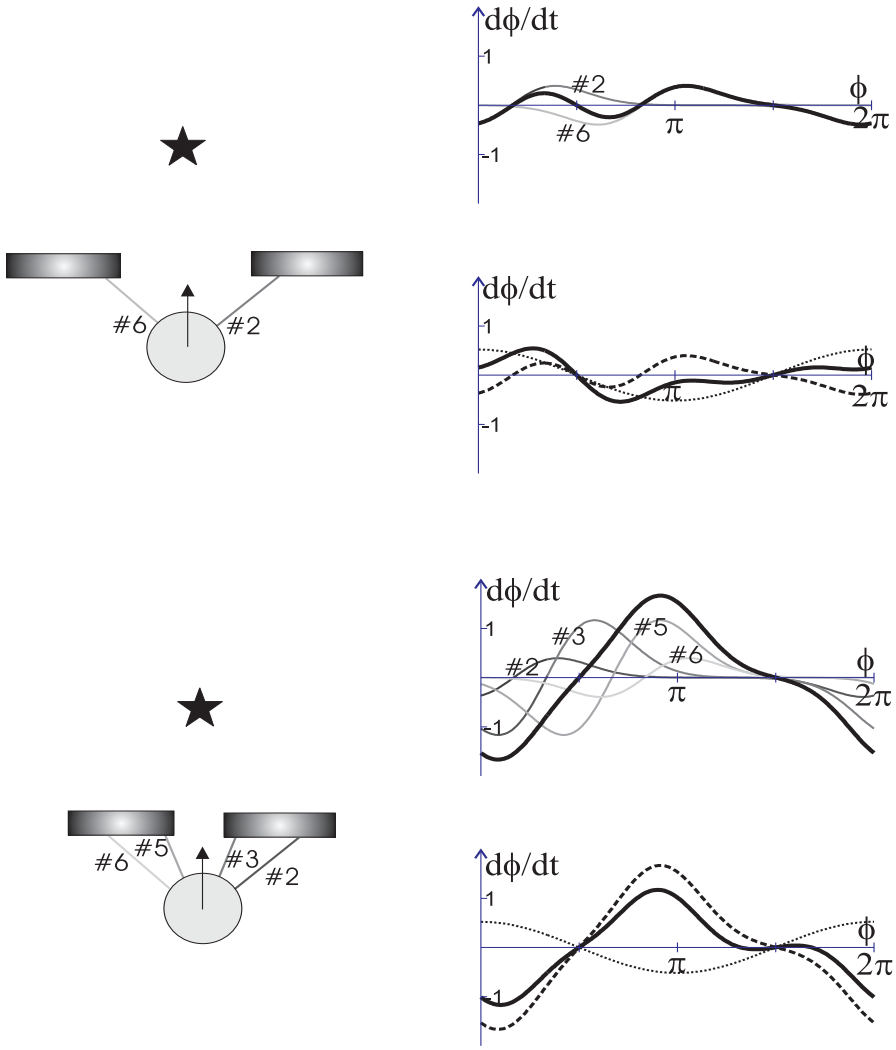

Figure 4.13: Demonstration of decision making by the path planning dynamics: The robot is placed at a distance 20 cm from the obstacles and facing them. The target lies behind the obstacles. The two pictures in the left column illustrate two situations: In the first (top of this column) the separation between the two obstacles is larger then the robot's size, while in the second (bottom of the column) the opposite holds. For each situation two plots are presented. The first plot shows the individual repulsive force-lets(grey lines) and their superposition (solid bold line). The second plot exhibits the resultant obstacles contribution (dashed line), target contribution (doted line) and the resultant dynamics of the heading direction (solid bold line). When the separation between the two obstacles is larger than the vehicle size the path planning dynamics forms an attractor at the direction pointing toward the passage. Conversely, the path planning dynamics erects a repeller at this direction when the distance between the obstacles is not sufficient for the robot to pass in between.

force-lets, which leads to a single repeller in the obstacle avoidance dynamics, positioned at their average location. These two obstacles (or four virtual obstacles) are thus behaviorally modeled as just one obstacle. The target contribution erects an attractor at that direction. However, since the repeller from the obstacle constraints is stronger than the attractor from the target constraint the resulting vector field keeps a repeller at that direction. Behaviorally this corresponds to the decision of steering away. Note that the resultant planning dynamics has two attractors, one on each side of the repeller, which reflect the two possibilities, turning right or left. If the robot turns left or right depends on which basin of attraction the heading direction is in. These decisions in the planning dynamics were investigated systematically for a continuum of distance values between obstacles ranging from 80 cm down to 0 cm when the robot is at a distance of 20 cm from the obstacles. The resulting fixed points are plotted in Figure 4.14 and their stability is indicated. When the obsta-

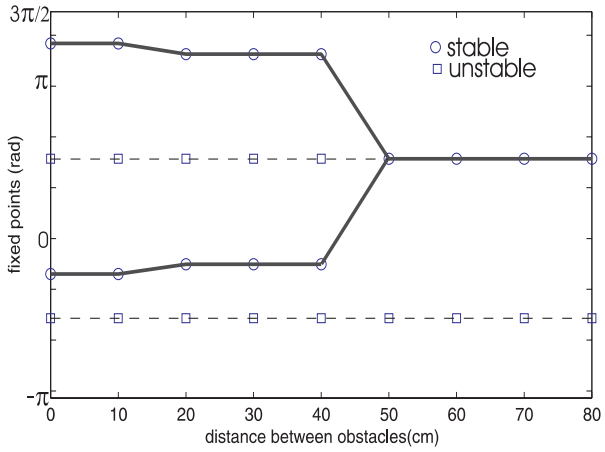

Figure 4.14: Bifurcation diagram of the path planning dynamics when the robot is at a distance of 20 cm from the obstacles. Stable and unstable fixed points are indicated by circles and squares, respectively. Pitch-fork bifurcation: The planning dynamics has an attractor at $\phi = \pi/2$ while the distance between obstacles is larger than 50 cm. For a distance value smaller than 50 cm this attractor becomes unstable (i.e. a repeller) and two new attractors appear. The value 50 cm is the bifurcation value and is the distance below which the vehicle (with size 45 cm) cannot pass between the two obstacles.

cles are 80 cm apart the planning dynamics exhibits an attractor at the direction in between the two obstacles. As the distance between obstacles is decreased a critical value is reached where a bifurcation in the planning dynamics takes place. This attractor becomes unstable and two new attractors appear (pitch-fork bifurcation[1]). The bifurcation point is at 50 cm and is the distance below which the robot (with size 45 cm) fails to pass physically between the two obstacles. Behaviorally, this bi-

[1]A bifurcation is called pitch-fork bifurcation when a stable fixed point becomes unstable and casts off two stable fixed points.

furcation leads to a qualitative change, i.e. a decision making, in the planned path. For distances larger than 50 cm the robot passes straight through the obstacles to reach the target while for smaller distances it turns around.

Decision making through bifurcations generated by the moving vehicle itself

The bifurcation we have just described was induced by changing the environment as sensed from the sensors, while the robot's position and orientation were kept fix. Now we show results where planning decisions arise during actual motion.

In Figure 4.15 the time course of the robot's position and corresponding planning dynamics, as the robot moves from an initial position toward the target location, is shown. The robot faces two obstacles that are separated by a distance (20 cm) smaller than the robot diameter. The target location lies behind the obstacles.

Initially (see Panel A) no obstructions are sensed by the infra-red sensors, thus the obstacle contributions to the vector field of the planning dynamics are null. Only the target contributes, the planning dynamics has therefore an attractor at the direction at which the target lies, as seen from the current position. The heading direction is relaxed in this attractor. As the robot approaches there is a distance for which it starts to detect obstructions (Panel B). The obstacle avoidance dynamics erects a repeller, at the average direction in between the two obstacles ($\pi/2$ rad), which is weakly repulsive since the obstacles are still far away. The resultant vector field maintains the attractor at about the same position although its strength of attraction is weakened. Behaviorally, the robot moves straight ahead. As the robot continues approaching the obstacles an instability takes place (Panel C). This because as the sensed distances to obstructions decrease the strength of the corresponding repulsive force-lets increase. Thus the strength of the repeller erected by the obstacle avoidance dynamics increases and eventually overrides the attractor, leaving a repeller there and two atractors, one on each side which correspond to the two possibilities, turning to the right or to the left. A bifurcation (subcritical pitch-fork bifurcation) in the path planning dynamics has taken place. The system has made a decision (no path is possible through the obstacles). As the distance decreases even further the strength of repulsion of this new repeller increases (Panel D) and strongly repels the heading direction of the robot from the direction it specifies. The robot circumnavigates then the entire area in which obstructions have been detected (Panel E). When it reaches the position indicated in Panel E another bifurcation takes place. An attractor replaces the repeller and the planning dynamics pulls henceforth the robot to move toward the target.

If there is no opening between the obstacles, so that a single broad obstruction is encountered (Figure 4.16), the same bifurcations take place and the robot follows a qualitatively similar path. A new challenge is posed however. When too many obstacle contributions are simultaneously activated, spurious attractors could hypothetically arise: the pull to the left exerted by one contribution could be cancelled by

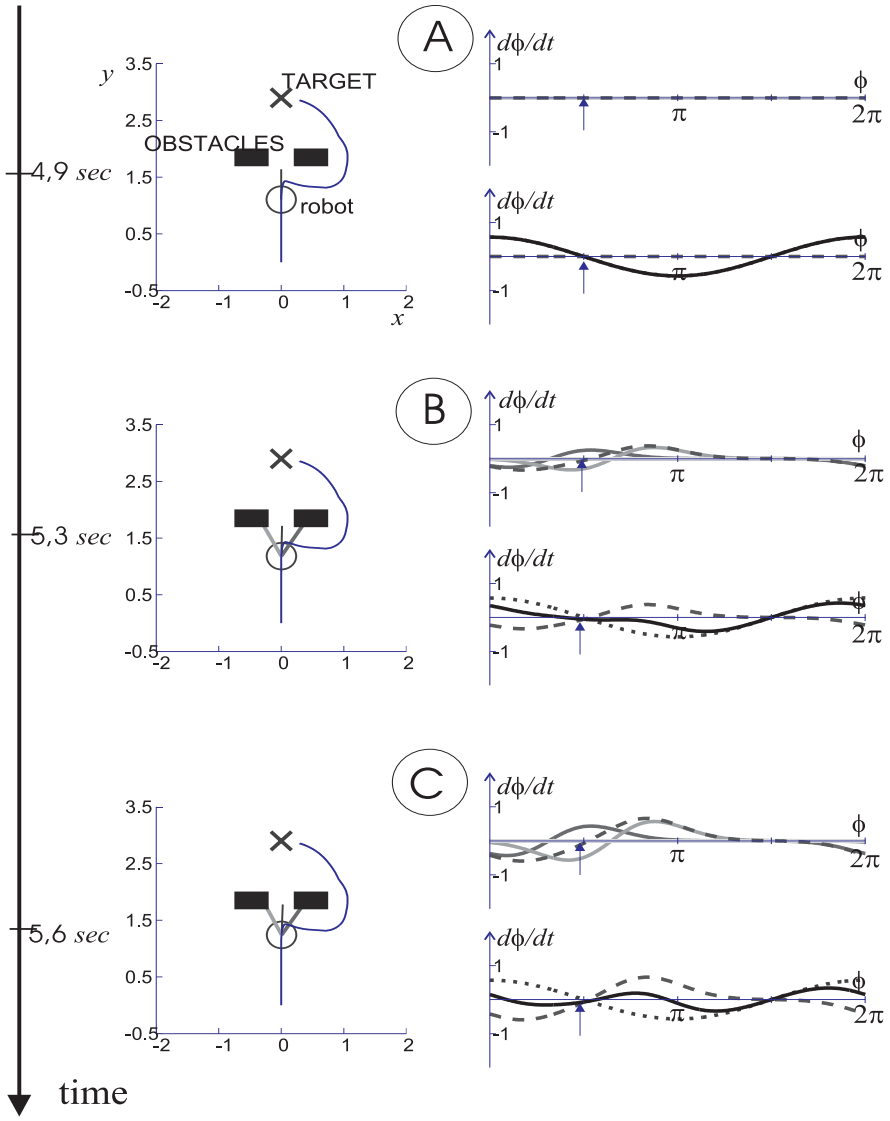

Figure 4.15: Evolution in time of the robot's position and corresponding heading direction dynamics as the robot moves toward the target. Initially the robot is positioned at coordinates $(0, 0)$ m facing two obstacles, which are separated by 20 cm (smaller than the vehicles size). The target position is at $(2.9, 0.0)$ m. Each picture in the left column shows the robot position at a certain instant of time. For each robot position two plots are presented. The first plot shows the individual repulsive force-lets (grey lines) and their superposition (dashed line). The second plot illustrates the resultant obstacle contributions (dashed line), the target contribution (doted line) and their sum (solid bold line). The arrow in the plots indicates the current value of the heading direction. The robot moves ahead, toward the target, until it detects the obstacles. Since the spacing between the obstacles is small the robot circumnavigates then both obstacles, through their right, and eventually reaches the target(cont.).

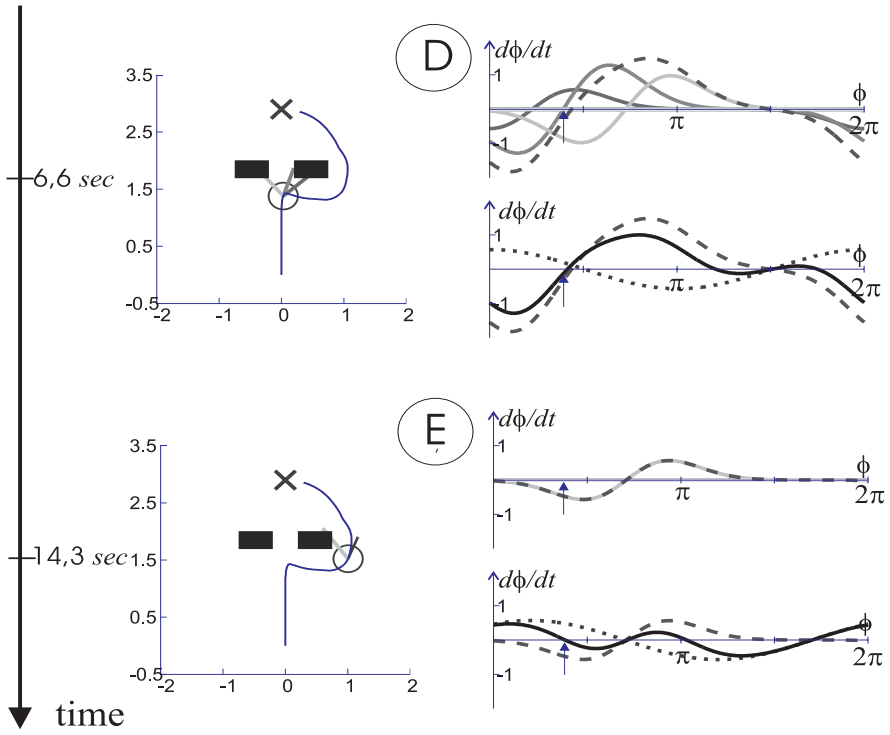

Figure 4.15: Continued.

the pull to the right of a next contribution. The figure demonstrates, however, that even when multiple contributions are simultaneously activated, spurious attractors need not arise.

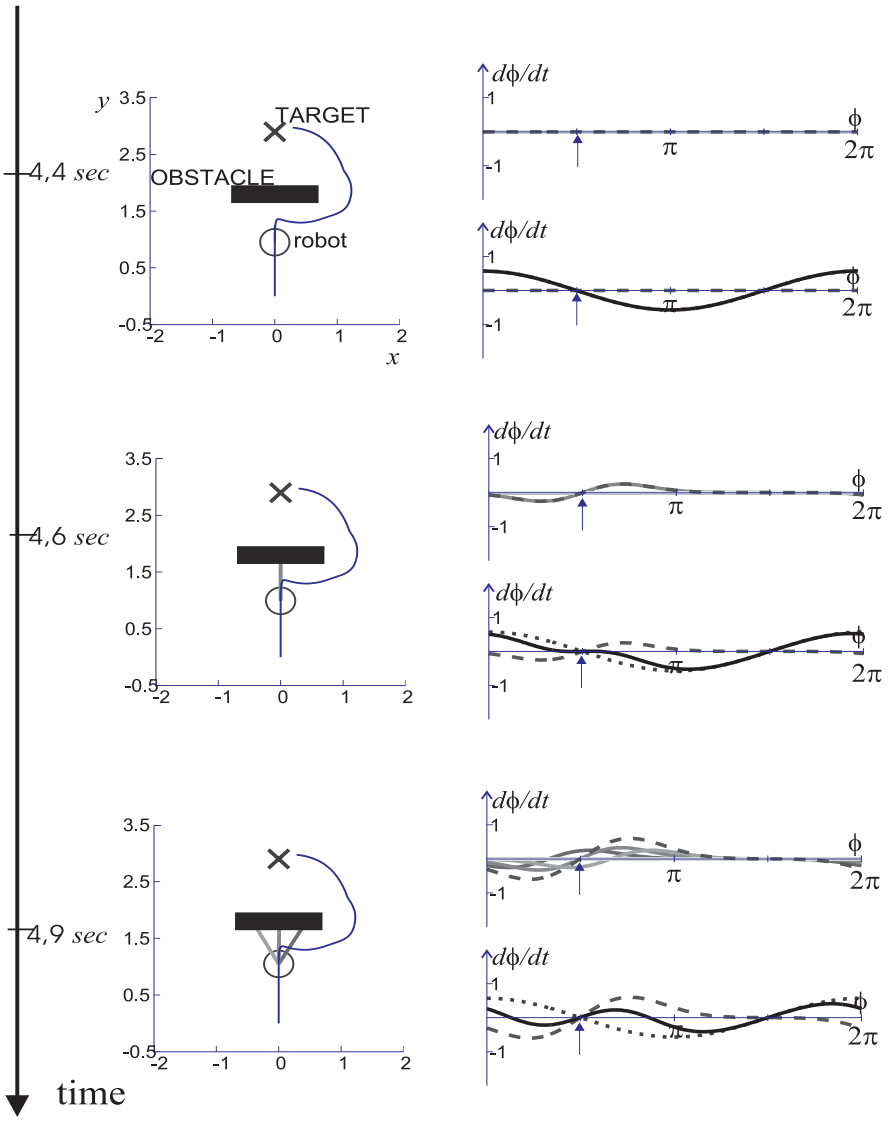

Figure 4.16: This figure is elaborated as explained in the Figure 4.15. The overture between the obstacles depicted in that figure is here closed. The robot follows a qualitative similar path. It circumnavigates the long obstacle and successfully reaches the target(cont.).

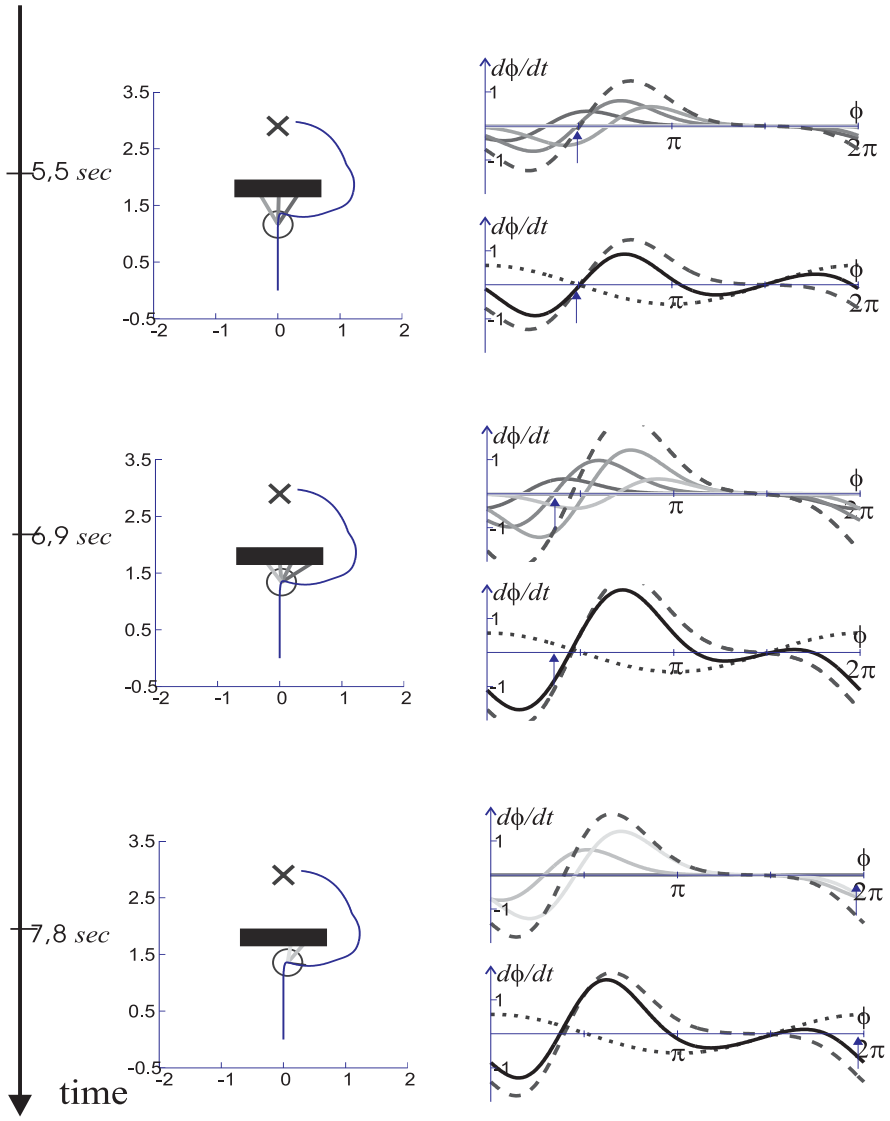

Figure 4.16: Continued.

When the separation between the obstacles is sufficiently large the path followed is qualitatively different. This is illustrated in Figure 4.17 where the overture between the two obstacles was made just slightly larger (55 cm) than the robot size. The time course of the robot position and corresponding planning dynamics is also depicted. While the distance of the robot to the obstacles is larger than the range of detection of the infra-red sensors no obstructions are detected and the resultant vector field has an attractor at the direction pointing toward the target (Panel A). The robot moves thus straight ahead. When the robot arrives at the position indi-

cated in Panel B it detects two obstructions. At this point the angular separation

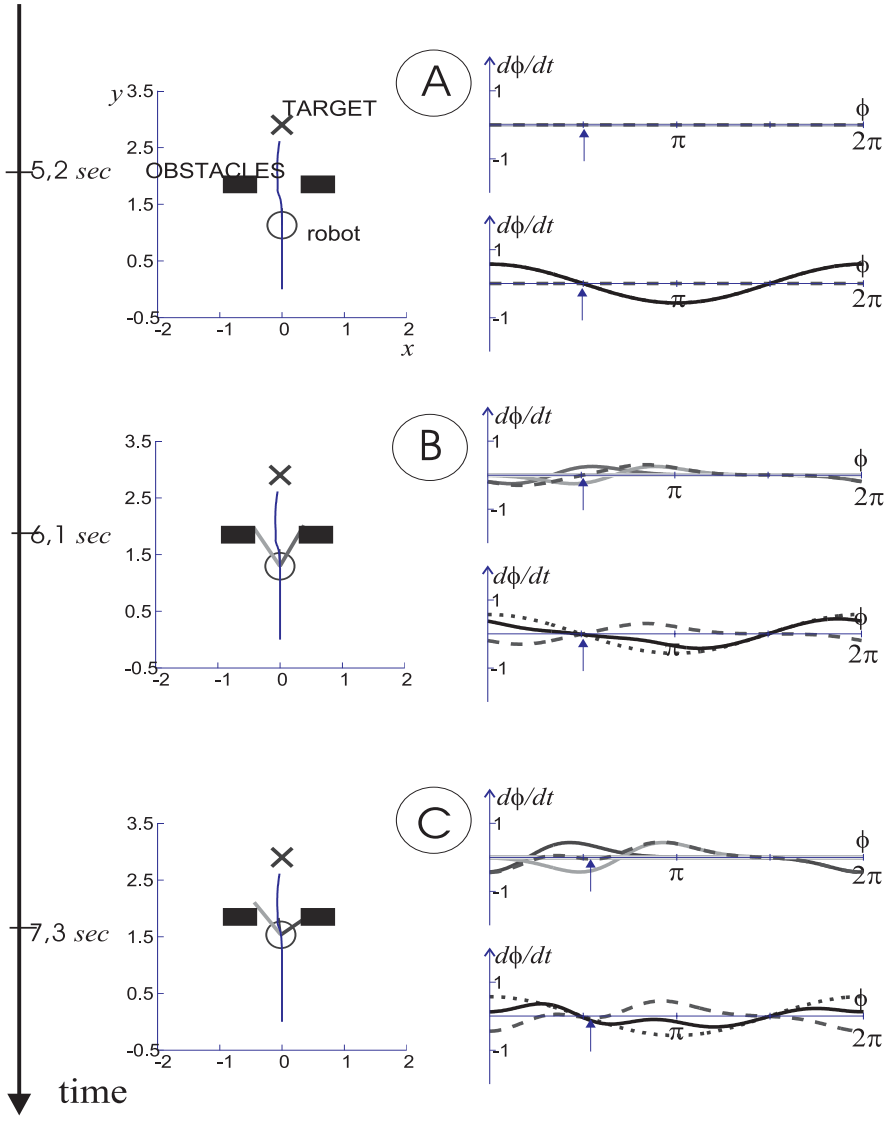

Figure 4.17: The obstacles depicted in Figure 4.15 are now placed at a distance of 55 cm which is larger than the robot's size. The qualitative path is therefore different. Here the path is more direct. The robot passes through the overture in between the obstacles to reach the target(cont.).

between the two obstructions, as detected from the current position of the robot, is relatively small. The corresponding repulsive force-lets are sufficiently overlapping and therefore these contributions are linearly dependent. Their superposition produces a repeller at their average angular distance. This repeller "competes" with the attractor from the target dynamics. Because the strength of the attractor is

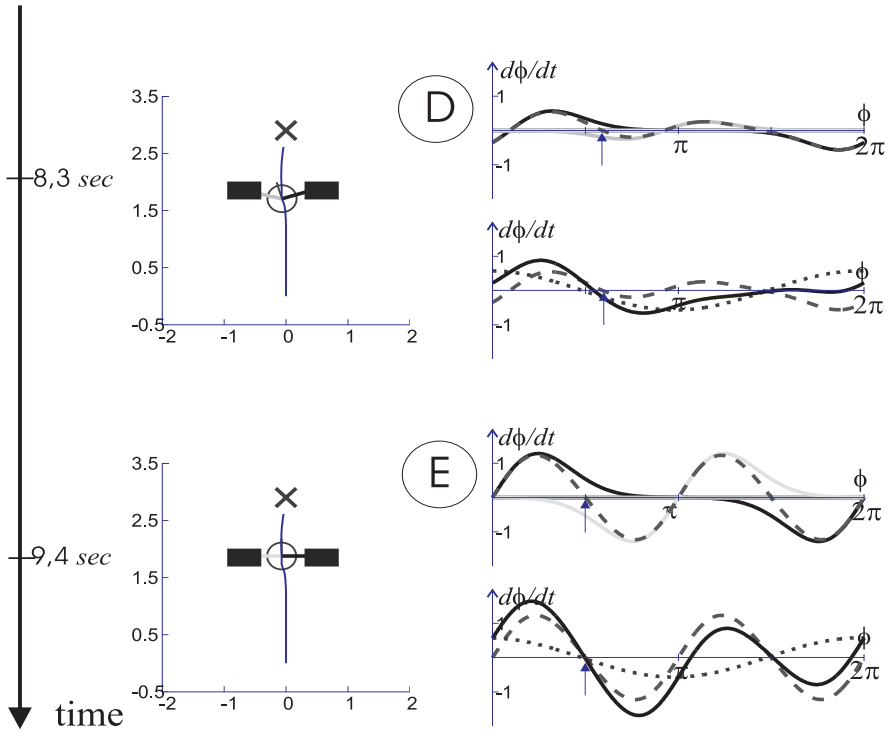

Figure 4.17: Continued.

stronger than the repulsion of the repeller the resultant vector field maintains an attractor, although less stable, at the direction at which the target is seen. The robot continues driving ahead. As the robot approaches the obstacles their angular separation, as detected from the current position of the robot, increases. The individual repulsive force-lets become less overlapping. At a certain distance a phase transition in the obstacle avoidance dynamics takes place. The sum of the repulsive contributions now forms an attractor at that direction (Panel C). From this point on, obstacle and target contributions cooperate and the resultant attractor is thus more stable. In spite of the fact that the obstacle dynamics went through a phase transition the complete vector field always produced a continuous varying attractor solution, which smoothly tuned the robot movement through the narrow passage toward the target.

Stability

We have just seen that as the vehicle moves the directions to the obstacles and the target in the world change, thus the resulting attractor of the planning dynamics shifts. Figure 4.18 shows, for the three examples presented above, how the time courses of the heading direction track the time courses of the attractor solutions of the heading direction dynamics. In each case, the system tracks one of the attractors closely, except for those moments in time, when a bifurcation occurs, and some time

is needed to relax to the nearest new attractor. These results demonstrate that the complete dynamic planning system is stably coupled in closed loop to the sensory information.

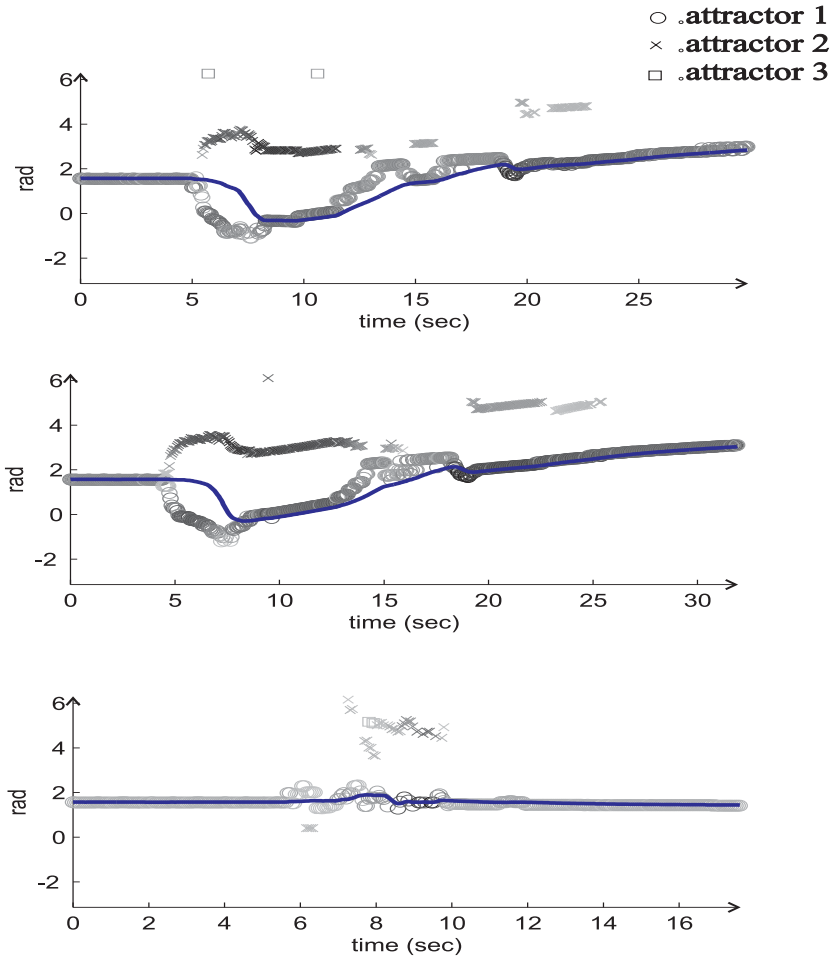

Figure 4.18: These three plots show the time course of the attractors and heading direction for each of the paths shown in Figures 4.15, 4.16 and 4.17 respectively. The attractors are represented by circles, crosses and squares. The color of these symbols gives information about the corresponding strength of attraction of the attractors they represent: The darker they are the more stable the attractors are. The time course of the heading direction is the black solid line.

4.5.2 Velocity control

To maintain the system stable, i.e. in or near an attractor, we guarantee that the vehicle drives sufficiently slow so that the rate of shift of the attractors occurs at a slower time scale than the time scale of the path planning dynamics. Figure 4.19

illustrates the path velocity dynamics as the sensed world changes.

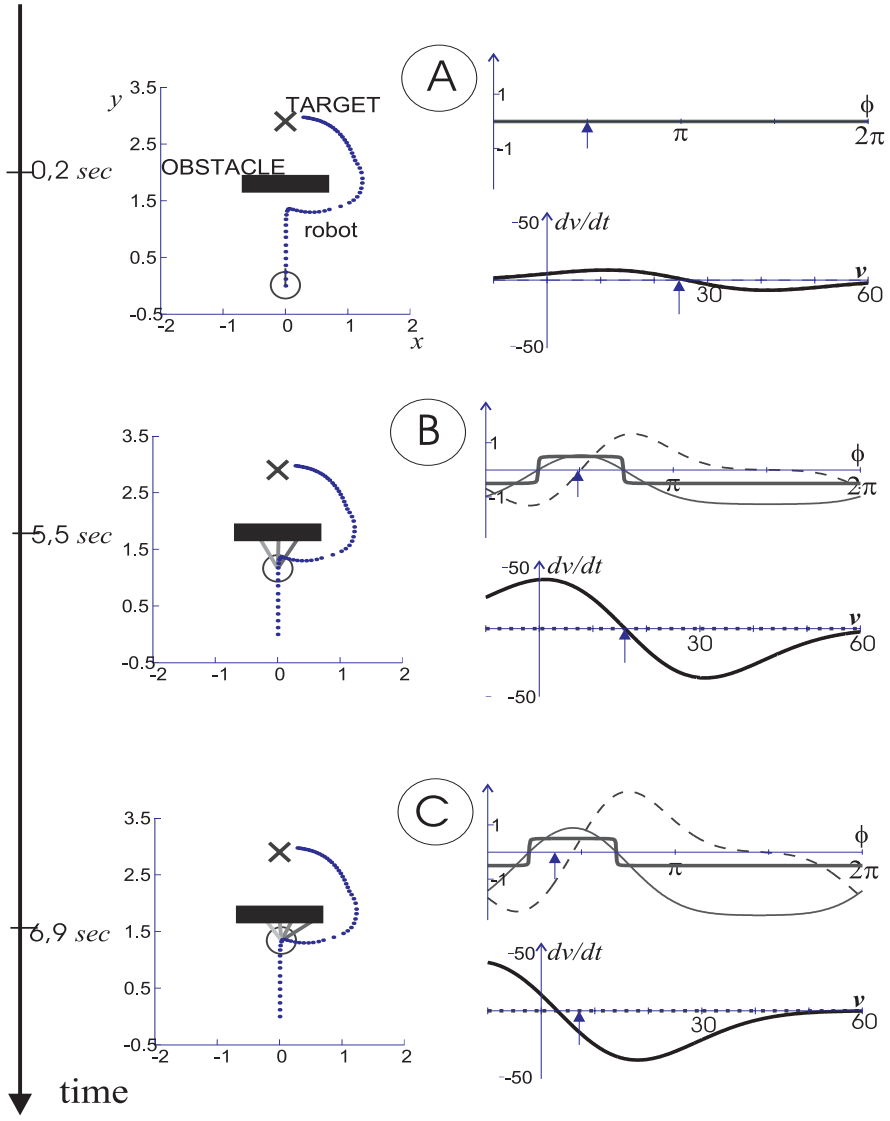

Figure 4.19: Evolution in time of the robot's position and velocity dynamics as the robot moves toward the target for the situation illustrated in Figure 4.16. Each picture in the left column shows the robot position at a certain instant of time. For each robot position two plots are presented. The first plot shows the resultant obstacle contributions F_{obs} (dashed line), the corresponding potential U (solid thin line) and thresholded potential α (solid bold line). The arrow indicates the current value of heading direction. The second plot depicts the velocity dynamics and the arrow indicates the vehicle's current velocity. The trajectory is depicted as a sequence of points. The time interval between two consecutive points of the trajectory is constant. Thus the plotted trajectory directly gives a perception of the robot's path velocity: The closer the points are the smaller the velocity is (cont.).

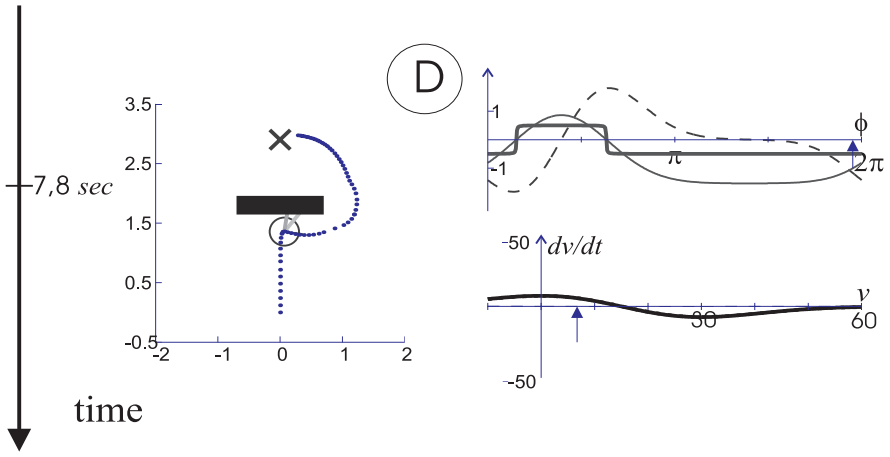

Figure 4.19: Continued.

Panel A shows that when no obstructions are detected (indicated by negative or zero $\alpha(\phi)$ at the current heading direction) the robot velocity is stabilized by an attractor, which is set proportional to the distance to the target, according to the target constraint imposed by Equation 4.15. Conversely when obstructions are detected (as illustrated in Panels B and C), $\alpha(\phi)$ is positive at the current heading direction, the velocity dynamics is governed then by an attractor whose value is proportional to the minimal sensed distance to the obstructions if this minimal distance is larger than 25 cm, otherwise its value is set proportional to $d_{\min} - 20$ cm. This way the obstacle constraints are satisfied. Panel D shows what happens in a situation where obstructions are detected but the robot's heading direction is outside the repulsion zone created by the obstructions ($\alpha(\phi)$ negative). In this case the velocity dynamics is dominated by the target constraint as we have just explained above. The strengths of the attractors, erected by target or obstacle contributions for the velocity dynamics, are adjusted according to Equation 4.21.

Again, as the vehicle moves the attractor for the path velocity dynamics, either erected by the target or obstacle constraints, shifts. The system is able to follow the attractor, however. This is depicted in figure 4.20.

4.5.3 Sample trajectories in complex environments

Figures 4.21 to 4.24 show sample trajectories of the robot as recorded by the dead-reckoned robot position. The initial position of the vehicle is always considered the referential point with respect to which the target coordinates $(X_{\text{target}}, Y_{\text{target}})$ are given. The vehicle stops running when the estimated distance to the center of the vehicle to the target is equal to 30 cm. The error in this estimated distance and the real distance varies between 10 and 20 cm depending on the length of the overall path.

In the run depicted in Figure 4.21 the robot is initially placed inside a box. The target position lies outside at coordinates $(X_{\text{target}}, Y_{\text{target}}) = (1.5, -1.5)$ m. As

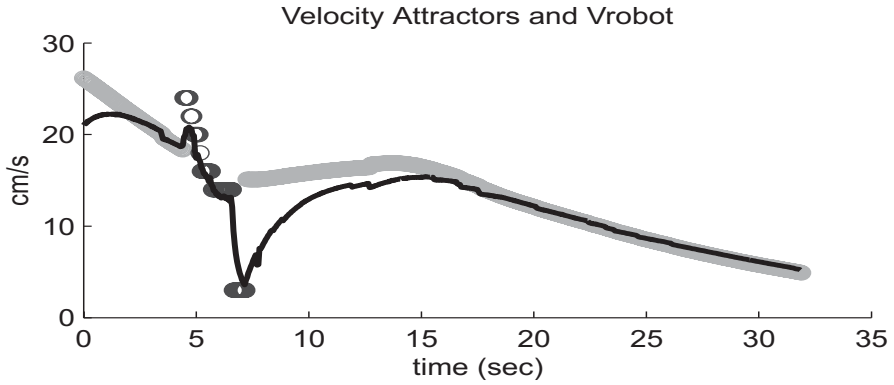

Figure 4.20: Time course of the attractor from the path velocity dynamics and robot's velocity along the path depicted in Figure 4.16. The attractor is represented by a circle. The color gives information about its strength of attraction. Darker color indicates stronger attractor. The time course of the path velocity is the black solid line.

one can see, the robot first turns toward the target direction and circumnavigates the detected obstacles that constitute the walls. It then finds the exit and continues moving toward the target until it is inside the neighborhood of the target coordinates.

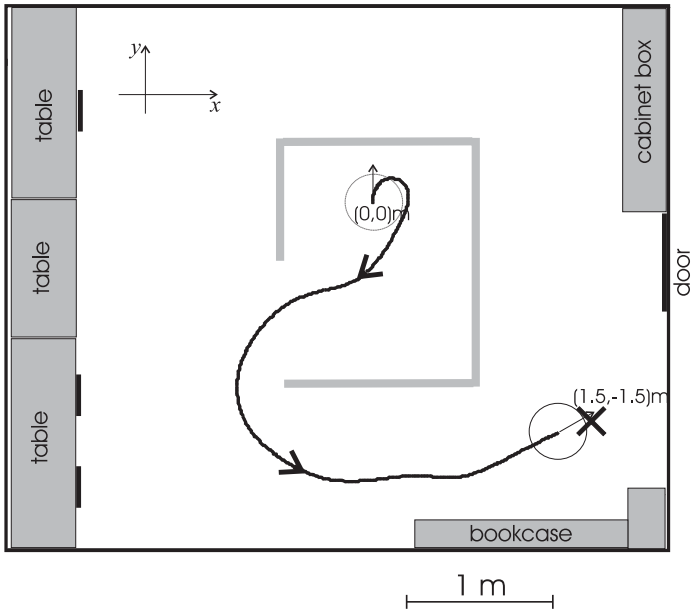

Figure 4.21: A sample trajectory of the robot as recorded by the dead-reckoned position. Robot initial position is considered the reference point. The target is placed at a position $(1.5, -1.5)$ m with respect the reference point.

The two runs depicted in Figure 4.22 demonstrate the flexibility of the path gen-

erating system. The results reported in subsection 4.5.1 have also demonstrated this property, of course, but here the environment is more complex. Initially the robot is positioned outside the box, in the bottom right corner. The target coordinates fall inside the box ($(X_{\text{target}}, Y_{\text{target}}) = (-2, 1.8)$ m). In the first run (top Panel) the robot circumnavigates the obstacles taking the top direction. It finds its way into the box while successfully avoiding the walls and finally ends up stopping near the target position. In the second run (bottom Panel) three obstacles indicated by A, have been placed in front of the robot with respect to its departure position. From this position the additional obstacles are not detectable, since they have been placed at a distance larger then the sensors range. Initially, the robot attempts to reach the target through the top direction as before. However, it detects that this way is a dead-end. Therefore, it changes the direction of driving and once again successfully reaches the target.

A longer run is illustrated in Figure 4.23. Initially, the robot is positioned in the corridor of our lab. The target position lies inside a box in one of the offices, $(X_{\text{target}}, Y_{\text{target}}) = (-3.2, 3.0)$ m. The robot drives along the corridor. Then, based on the target contribution and helped by obstacle avoidance, the robot moves through the office door. It circumnavigates the obstacles and eventually reaches the entrance of the box. Finally, it stops near the target position.

All the results presented till now were obtained using distance measures provided by infra-red sensors only, because it makes the computation cycle faster and thus larger path velocities are possible. We end this section by illustrating the simultaneous use of infra-red sensors and sonars and the concomitant implications in the generated path.

When infra-red sensors are used together with the sonars, sensory information is acquired in the following way: The signal of each infra-red sensor is read only once per each computation cycle as when they are used in isolation. In each computation cycle five measures for each sonar are taken. In this case the cycle time is approximately 70 ms. The distance estimate provided by a sonar is then taken as the average among the five measures. This way errors due to specular reflexions are reduced to a large extend. The "sensory fusion" between infra-red sensors and sonars is performed through a very simple algorithm. In the overlap distances interval (e.g from 45 to 60 cm) the minimum distance is taken as the estimated distance to a detected obstruction.

Figure 4.24 illustrates how sensors distance range affect the generated path. This figure shows two runs executed in the same scenario. The target position is at coordinates $(X_{\text{target}}, Y_{\text{target}}) = (-1.0, 2.2)$ m with respect to the vehicle's departure position. In the first run only infra-red sensors have been used to measure distances to obstructions. The maximal distance at which obstructions can be detected is 60 cm. Initially, the robot turns left in order to avoid the obstacles, indicated by A, which lie on its right side. Then the robot attempts to reach the target through the left direction. However it detects that this way is a dead-end (indicated by B). It changes therefore its direction of driving and successfully reaches the target position.

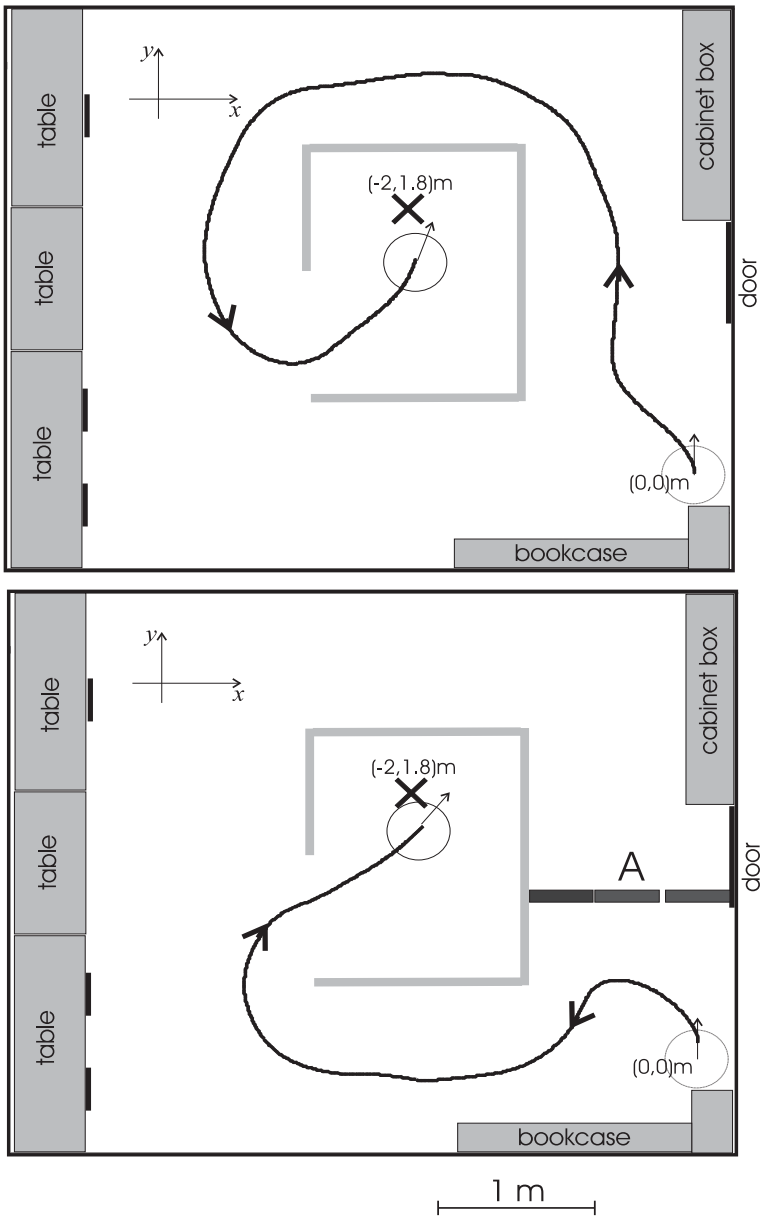

Figure 4.22: Flexibility of the path generating system is illustrated here. Top: the robot is positioned initially at the lower left corner as illustrated. The target lies inside the box at coordinates $(-2, 1.8)$m with respect to the departure position. The generated trajectory that brought the system from its initial position to the target location is depicted. Bottom: Here additional obstacles have been added to the configuration in a form that blocks the previous path. The resultant trajectory takes a different course.

In the second run (depicted on the right side of the figure) both infra-red sensors and sonars are used. The maximal distance at which obstructions can be detected is now 175 cm. The robot starts detecting obstacles for larger distances and as a

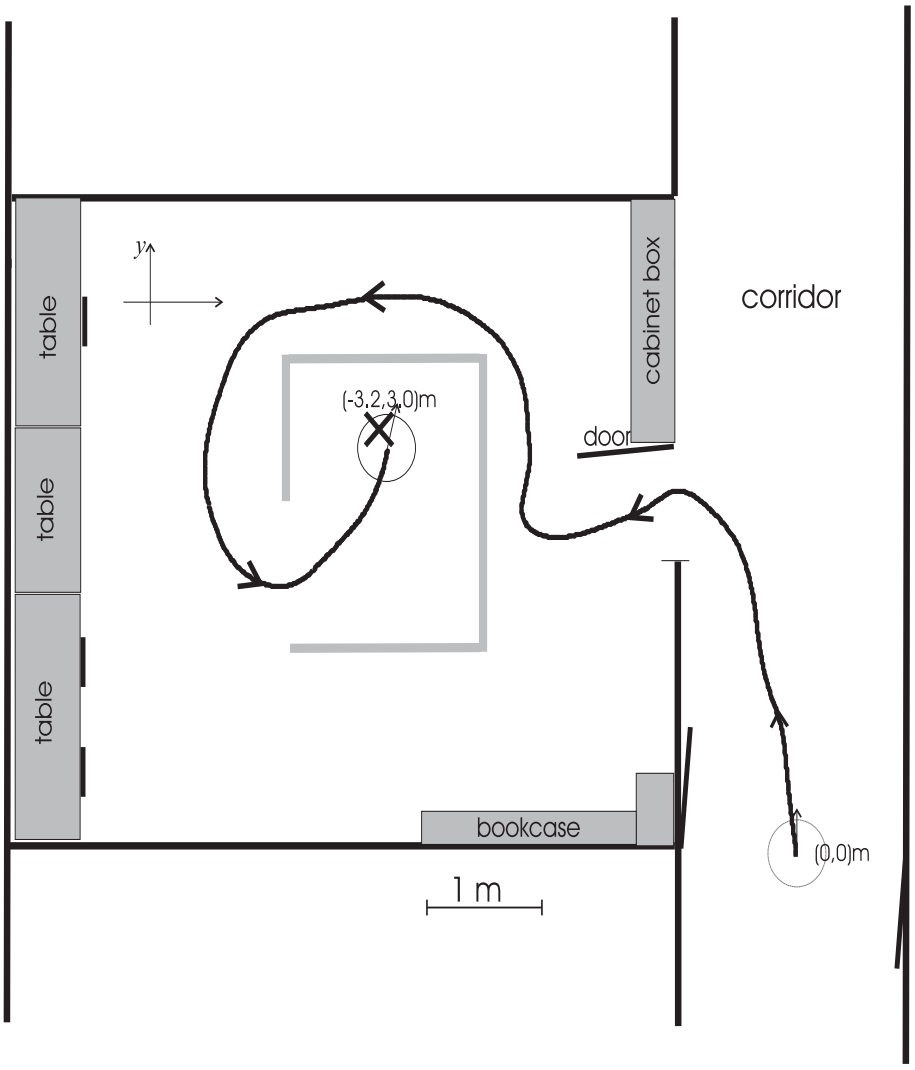

Figure 4.23: Another and longer trajectory is depicted here. The robot is initially placed at the corridor. The target location is inside an office at coordinates $(-3.2, 3)$m relative to the departure position.

consequence it can anticipate which direction to move. The dead-end is detected earlier.

As we can see from the results the dynamic path planning system leads to smooth collision free trajectories to the target. The result is valid for both types of sensors.

4.6 Conclusion

In this chapter we have demonstrated that the dynamic approach to path generation can be used even in the absence of veridical representations of obstacles as objects

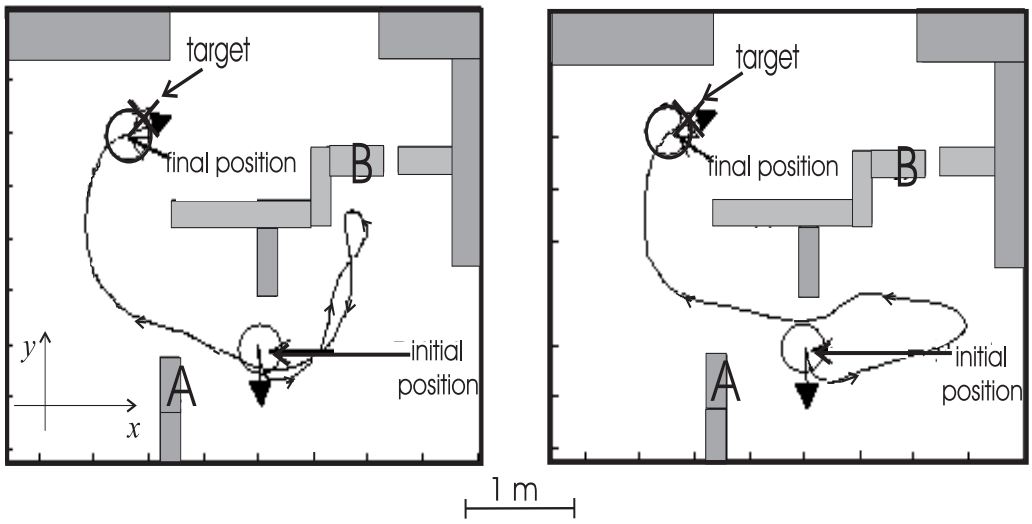

Figure 4.24: Two sample trajectories of the vehicle as recorded by the dead-reckoned position are depicted. The target is placed at coordinates $(-1.0, 2.2)$ m with respect to the robot's initial position. Left: Only infra-red sensors have been used to measure distances to obstructions. Right: Distance measures to obstructions have been provided by infra-red sensors and sonars.

in the world. The information from distance sensors is directly used to define contributions to a dynamical system of path planning. Heuristically, the sum over such contributions has attractors that specify collision free directions toward the target. Target and obstacle constraints also define contributions to a dynamical system of path velocity. The generated trajectories are smooth. Flexibility is achieved in that as the sensed environment changes, the system may change its planning solution continuously, but also discontinuously.

Because this dynamic path generation system is a local form of path planning one cannot guarantee that the trajectories toward a target are optimal with respect to the overall traveled path.

The proposed solution involves explicit design and all system parameters can be specified rationally based on the qualitative theory of dynamical systems and bifurcation theory. The system never entered into spurious attractors.

Although we did not show here it for technical reasons, the dynamic architecture works for dynamic environments, as long as the rate of change of the environment is slow compared with the relaxation time of the planning dynamics. No conceptual difference exists between stationary and moving obstacle avoidance. Avoiding moving obstacles is shown on a video demonstration.

Since motion planning is just a piece in the way robots interact with their world, a next direction is to integrate this motion planning system with the related problem of target detection and localization.

Bibliography

[1] S Amari. Dynamics of pattern formation in lateral-inhibition type neural fields. *Biological Cybernetics*, 27:77–87, 1977.

[2] Y Ando, T Tsubouchi, and S Yuta. A reactive wall following algorithm and its behavior of an autonomous mobile robot with sonar ring. *Journal of Robotics and Mechatronics*, 8(1):79–86, 1996.

[3] R C Arkin. Motor schema-based mobile robot navigation. *The International Journal of Robotics Research*, 8(4):92–112, 1989.

[4] R C Arkin. *Behavior-Based Robotics*. MIT Press, Cambridge, 1998.

[5] C Balkenius. *Natural Intelligence in Artificial Creatures*. Lund University Cognitive Studies, 37, 1995.

[6] J Barraquand and J-C Latombe. Robot motion planning: a distributed representation approach. *The International Journal of Robotics Research*, 10, 1990.

[7] G Bauzil, M Briot, and P Ribes. A navigation subsystem using ultrasonic sensors for the mobile robot Hilary. In *First Int. Conf. on Robot Vision and Sensory Control*, pages 47–58, Stratford–upon–Avon, UK, 1981.

[8] R D Beer. A dynamical systems perspective on agent-environment interaction. *The AI Journal*, 72:173–215, 1995.

[9] T Bergener, C Bruckhoff, P Dahm, H Janssen, F Joublin, R Menzner, A Steinhage, and W von Seelen. Complex behavior by means of dynamical systems for an anthropomorphic robot. In *Organization of Computation in Brain-like Systems, 1999 Special Issue of Neural Networks*, October 1999.

[10] T Bergener and A Steinhage. An architecture for behavioral organization using dynamical systems. In C Wilke, S Altmeyer, and T Martinetz, editors, *Abstracting and Synthetesizing the Principle of Living Systems: Proceedings of the Third German Workshop on Artificial Life*, pages 31–42. Verlag Harri Deutsh, 1998.

[11] E Bicho, P Mallet, and G Schöner. Using attractor dynamics to control autonomous vehicle motion. In *Proceedings of the 24th Annual Conference of the IEEE Industrial Electronics Society (IECON98)*, pages 1176–118, Aachen-Germany, Aug/Set IEEE, Piscataway, NJ, 1998.

[12] E Bicho, P Mallet, and G Schöner. Target representation on an autonomous vehicle with low-level sensors. *International Journal of Robotics Research, in press*, 1999a.

[13] E Bicho, P Mallet, and G Schöner. Using attractor dynamics to control autonomous vehicle motion. *IEEE Transaction on Robotics and Automation, submitted*, 1999b.

[14] E Bicho and G Schöner. The dynamic approach to autonomous robotics demonstrated on a low-level vehicle platform. *Robotics and autonomous systems*, 21:23–35, 1997a.

[15] E Bicho and G Schöner. Target position estimation, target acquisition, and obstacle avoidance. In *Proceedings of the IEEE International Symposium on Industrial Electronics (ISIE'97)*, pages SS13–SS20. IEEE, Piscataway, NJ, 1997b.

[16] J Blauert. *Spatial Hearing - The Psychophysics of Human Sound Localization.* MIT Press, Cambridge MA, USA, 1996.

[17] J Borenstein and Y Koren. Real-time obstacle for fast mobile robots. *IEEE Transactions on Systems, Man and Cybernerics*, 19(5):1179–1187, Sep/Oct 1989.

[18] V Braitenberg. *Vehicles. Experiments in Synthetic Psychology.* MIT Press, Cambridge, Mass., 1984.

[19] R W Brockett. Asymptotic stability and feedback stabilization. In *Differential Geometric Control Theory*, number ISBN 3-7643-3091-0. Birkhäuser, 1983.

[20] R A Brooks. Solving the find-path problem by good representations of free space. *IEEE Transactions on Systems, Man and Cybernetics*, SMC-13(3):190–197, March-April 1983.

[21] R A Brooks. A robust layered control system for a mobile robot. *IEEE Journal of Robotics and Automation*, RA-2:12–23, 1986.

[22] R A Brooks. A robot that walks: Emergent behavior from a carefully evolved network. *Neural Computation*, 1(2):253–262, 1989.

[23] R A Brooks. Intelligence without representation. *Artificial Intelligence*, 47:139–160, 1991.

[24] R A Brooks. New approches to robotics. *Science*, 253:1227–1232, 1991.

[25] R A Brooks. Artificial life and real robots. In F J Varela and P Bourgne, editors, *Towards a Practice of Autonomous Systems: Proceedings of the first European Conference on Artficial Life*. The MIT Press, 1992.

[26] R A Brooks. From earwigs to humans. *Robotics and Autonomous Systems*, 20:291 – 304, 1997.

[27] R A Brooks and J H Connell. Asynchronous distributed control system for a mobile robot. *SPIE, Mobile Robots*, 727:77–84, 1986.

[28] C Bruckhoff and P Dahm. Neural fields for local path planning. In *Proceedings of the International Conference on Intelligent RObotic Systems (IROS 98)*, pages 1431–1436, October 1998.

[29] W H Cade and E S Cade. Male mating sucess, calling and searching behavior at high and low densities in the field cricket, gryllus integer. *Animal Behavior*, 43:49–56, 1992.

[30] S Cameron. Motion planning and collision avoidance with complex geometry. In *IECON 98, 24th Annual Conference of the IEEE Industrial Electronics Society*, volume 2, pages 2222–2226, Aachen-Germany, Aug 31 - Sep 4 1998.

[31] R Chatila. Representations + reason + reaction → robot intelligence. In T Kanade and R Paul, editors, *Robotics Research — Tthe Sixth International Symposium*, pages 387–397. The International Foundation for Robotics Research, Cambridge, MA, U.S.A., 1994.

[32] T M Chen and R C Luo. Development and integration of multiple behaviors for autonomous mobile robot navigation. In *IECON 98, 24th Annual Conference of the IEEE Industrial Electronics Society*, volume 2, pages 1146–1151, Aachen-Germany, Aug 31 - Sep 4 1998.

[33] R Chipalkatti and M A Arbib. The prey localisation model: A stability analysis. *Biological Cybernetics*, 57:287–299, 1987.

[34] J H Connell. *Minimalist Mobile Robotics*. Academic Press, 1990.

[35] C I Connolly, J B Burns, and R Weiss. Path planning using Lapalce's equation. *IEEE Robotics and Automation*, pages 2102–2106, 1990.

[36] I Cox. Blanche-an exprimental in guidance and navigation of an autonomous robot vehicle. *IEEE Transactions on Rotocis and Automation*, 7(2):193–204, 1991.

[37] I J Cox and G T Wilfong, editors. *Autonomous robot vehicles*. Springer Verlag, Berlin, 1990.

[38] J D Crawford. Introduction to bifurcation theory. *Reviews of Modern Physics*, 63(4):991–1037, 1997.

[39] P Dahm and C Bruckhoff. Autonomous decision making in local navigation. In *From Animals to Animats 5: Proceedings of the Fifth International Conference on Simulation of Adaptive Behavior (SAB 98)*, pages 229–233. MIT Press, August 1998.

[40] P Dahm, C Bruckhoff, and F Joublin. A neural field approach to robot motion control. In *Proceedings of the 1998 IEEE International Conference on Systems, Man, and Cybernetics (SMC'98)*, pages 3460–3465, 1998.

[41] O Duda. Auditory localization demonstrations. *Acustica - Acta Acusticca*, 82(2):346–355, Mar 1996.

[42] C Engels and G Schöner. Dynamic fields endow behavior-based robots with representations. *Robotics and autonomous systems*, 14:55–77, 1995.

[43] W Erlhagen. *Lokalisierte, stationäre Verteilung in neuronalen Feldern (Localized stationary distribuitions in neural fields)*. Harri Deutsch, Frankfurt, 1997.

[44] J P Ewert. The neural basis of visually guided robots. *Sci. Am.*, 230:34–42, 1974.

[45] D Feng and B Krogh. Satisficing feedback strategies for local navigation of autonomous mobile robots. *IEEE Transactions on Systems, Man and Cybernetics*, 20(6):476–488, November-December 1990.

[46] A Fujimori, P N Nikiforuk, and M M Gupta. Adaptive navigation of mobile robots with obstacle avoidance. *IEEE Transactions on Robotics and Automation*, 13(4):596–602, August 1997.

[47] M A Giese. *Dynamic neural model for motion perception*. Kluwer Academic, 1999.

[48] G Giralt. An integrated navigation and motion control system for autonomous multisensory mobile robots. pages 191–214. The International Foundation for Robotics Research, Cambridge, MA, U.S.A., 1984.

[49] G Giralt. Robot autonomoy and mashine intelligence: Trends and critical issues — A post-symposium report. In T Kanade and R Paul, editors, *Robotics Research — Tthe Sixth International Symposium*, pages 363–370. The International Foundation for Robotics Research, Cambridge, MA, U.S.A., 1994.

[50] K Y Guentchev and J Weng. Learning-based three dimensional sound localization using a coplanar array of microphones. In *Intelligent Environments Symposium*, Proc. 1998 AAAI Spring Symposium Series, Stanford University, Mar 23-25 1998.

[51] D H House. A model of the visual localization of prey by frog and toad. *Biological Cybernetics*, 58:173–192, 1988.

[52] H Hu and M Brady. Dynamic path planning with uncertainty for mobile robots in manufacturing. *IEEE Transactions on Robotics and Automation*, 13(5):760–766, October 1997.

[53] J Iijima, S Yuta, and Y Kanayama. Elementary functions of a self-contained robot YAMABICO 3.1. In S J et al. Hanson, editor, *Proc. 11th Int. Symp. Ind. Robots*, pages 211–218, Tokyo, 1993. The MIT Press.

[54] J Jones and A M Flynn. *Mobile Robots – Inspiration to implementation.* A K Peters, 289 Linden Str., Wellesley, MA 02181 USA, 1993.

[55] K Kedem and M Sharir. An automatic motion planning system for a convex polygonal mobile robot in 2-dimensional polygonal space. In *Proceedings of the 4th Annual Symposium on Computational Geometry*, pages 239–340. Association for Computing Mashinery, 1988. reprinted in Cox and Wilfong (eds.) (1990).

[56] O Khatib. Real-time obstacle avoidance for manipulators and mobile robots. *International Journal Robotics Research*, 5:90–98, 1986.

[57] B K Kim and K G Shin. Minimum-time path planning for robot arms and their dynamics. *IEEE Transactions on Systems, Man and Cybernetics*, SMC-15(2):213–223, 1985.

[58] K Kishimoto and S Amari. Existence and stability of local excitations in homogeneous neural fields. *Journal of Mathematical Biology*, 7:303–318, 1979.

[59] K Kopecz and G Schöner. Saccadic motor planning by integrating visual information and pre-information on neural, dynamic fields. *Biological Cybernetics*, 73:49–60, 1995.

[60] D Y Kortenkamp, R P Bonasso, and R Murphy. *Artificial Intelligence and Mobile Robots.* AAAI Press, Cambridge, 1998.

[61] J R Koza. Evolution of a subsumption architecture that performs a wall following task for an autonomous mobile robot. In S J et al. Hanson, editor, *Computational Learning Theory and Natural Learning Systems.* The MIT Press, 1994.

[62] Y Kuwana and I Shimoyama. A pheromone-guided mobile robot that behaves like a silkworm moth with living antennae as pheromone sensors. *International Journal of Robotics Research*, 17(9):924–933, 1998.

[63] E W Large, H I Christensen, and R Bajcy. Scaling the dynamic approach to path planning and control: Competition amoung behavioral constraints. *International Journal of Robotics Research*, 18(1):37–58, 1999.

[64] J C Latombe. *Robot Motion Planning*. Kluwer Academic Publishers, 1991.

[65] J P Laumond. Motion planning for mobile robots: From academic to practical issues. In *Robotics Research, the sixth International Symposium, The International Foundation for Robotics Research*, pages 21–27, Cambridge, USA, 1993.

[66] M Liggins, I Kadar, and V Vannicola. Distributed fusion architectures and algorithms for taeget tracking. In *Proc. of the IEEE*, volume 85, January 1997.

[67] T Lozano-Perez and W A Wesley. An algorithm for planning collision free paths among polyhedral obstacles. *Communications of the Association for Computing Mashinery ACM*, 22(10), 1979.

[68] V J Lumelsky and A A Stepanov. Dynamic path planning for a mobile automaton with limited information on the environment. *IEEE Transactions on Automatic Control*, AC-31(11):1058–1063, November 1986.

[69] V J Lumelsky and A A Stepanov. Path planning strategies for a point mobile automation moving amidst unknown obstacles of arbitrary shape. *Algorithmica*, 1987.

[70] H H Lund, B Webb, and J Hallam. A robot attracted to the cricket species *Gryllus bimaculatus*. In P Husbands and I Harvey, editors, *Fourth European Conference on Artificial Life*, pages 246–255. MIT Press, 1997.

[71] H Mallot, H Bülthoff, J J Little, and S Bohrer. Inverse perspective mapping simplifies optical flow computation and obstacle detection. *Biological Cybernetics*, 64:172–185, 1991.

[72] M J Mataric. A distributed model for mobile mobile robot environment-learning and navigation. In *Technical report, AI-TR-1288*, MIT Artficial Intellligence Laboratory, 1990.

[73] M J Mataric. Behavior-based control: Main properties and implications. In *Proceedings of Workshop on Intelligent Control Systems, International Conference on Robotics and Automation*, pages 169–175, Nice, France, May 1992.

[74] M J Mataric. Behavior-based robotics as a tool for synthesis of artificial behavior and analysis of natural behavior. *Trends in Cognitive Sciences*, 2(3):82 – 87, 1998.

[75] J McCarthy, M Minsky, N Rochester, and C Shannon. A proposal for the darthmounth summer research project on artificial intelligence. August 1955.

[76] Q Meng, D Liu, M Zhang, and Y Sun. Wall-following by an autonomously guided vehicle (agv) uisng a new-fuzzy-I(integration) controller. *Robotica*, 17:79–86, 1999.

[77] A Mills. Auditory localization. *Foundations of Modern Auditory Theory*, 2:301–348, 1972.

[78] H Neven. *Dynamics for vision-guided autonomous mobile robots*. Fortschrittberichte, Düsseldorf, 1997.

[79] H Neven and G Schöner. Neural dynamics parametrically controlled by image correlations organize robot navigation. *Biological Cybernetics*, 75:293–307, 1996.

[80] N J Nilson. A mobile automation: An application of artficial intelligence techniques. In *Proceedings of 1st Int. Joint Conf. on Artificial Intelligence*, pages 509–520, washigton, DC, 1969.

[81] L Perko. *Differential Equations and Dynamical Systems*. Springer Verlag, Berlin, 1991.

[82] A Pruski. Robots mobiles autonomes. *Traité Mésures et Contrôle des Techniques de l'Ingénieur*, R7(850):1–18, 1999.

[83] E Rimon and D E Koditschek. Exact robot navigation using artificial potential functions. *IEEE Transactions on Robotics and Automation*, 8(5):501–518, 1992.

[84] S J Ross, J M Daida, C M Doan, T F B Begey, and J McClain. Variations in evolution of subsumption architectures using genetic programming: The wall following robot revisited. In JR Koza, D E Goldberg, D B Fogel, and Riolo R L, editors, *Proceedings of the First Annual Conference*, July 1996.

[85] E R Scheinerman. *Invitation to Dynamical Systems*. Prentice Hall, 1996.

[86] H Schöne. *Spatial Orientation – The spatial control of behavior in animals and man*. Princeton University Press, Princeton, NJ, 1984.

[87] G Schöner and M Dose. A dynamical systems approach to task-level system integration used to plan and control autonomous vehicle motion. *Robotics and Autonomous Systems*, 10:253–267, 1992.

[88] G Schöner, M Dose, and C Engels. Dynamics of behavior: Theory and applications for autonomous robot architectures. *Robotics and Autonomous Systems*, 16:213–245, 1995.

[89] J T Schwartz and M Sharir. On the piano movers' problem: I. the case of a two-dimensional rigid polygonal body moving amidst polygonal barriers. *Communications in Pure and Applied Mathematics*, 36:345–398, 1983.

[90] S Shama, N Shen, and P Gopalawamy. Stereausis: Binaural processing without neural delays. *Journal of the Acoustical Society of America*, 86:989–1006, Mar 23-25 1989.

[91] K.G. Shin and N. D. McKay. Minimum-time control of robotic manipulators with geometric path constraints. *IEEE Transactions on Automation and Control*, AC-30(6):531–541, June 1985.

[92] J S Singh and M D Wagh. Robot path planning using intersecting convex shapes. *IEEE Transactions on Robotics and Automation*, RA-3:101–108, 1987.

[93] T Smithers. What the dynamics of adaptive behaviour and cognition might look like in agent-environment systems. In *Presented at the workshop: On the Role of Dynamics in Representation in Adaptive Behaviour and Cognition, 9/10 December 94, San Sebastian, Spain*, 1994.

[94] A Steinhage. *Dynamical Systems for the Generation of Navigation Behavior*. Shaker Verlag, Aachen, 1998.

[95] A Steinhage and G Schöner. Self-calibration based on invariant view recognition: Dynamic approach to navigation. *Robotics and Autonomous Systems*, 20:133–156, 1997.

[96] R Takahashi and R J Schilling. Motion planning in a plane using generalized voronoi diagrams. *IEEE Transactions on Robotics and Automation*, 5(2):143–150, April 1989.

[97] P Turennout, G Honderd, and L J Schelven. Wall-following control of a mobile robot. In *Proceedings of the 1992 IEEE International Conference on Robotics and Automation*, pages 280–285, Nice, France, May 1992.

[98] W G Walter. *The living brain (reprinted 1963)*. Norton, New York, 1953.

[99] B Webb. Using robots to model animals: a cricket test. *Robotics and Autonomous Systens*, 16:117–134, 1995.

[100] H R Wilson and J D Cowan. A mathematical theory of the functional dynamics of cortical and thalamic nervous tissue. *Kybernetik*, 13:55–80, 1973.

[101] T Yata, L Kleeman, and S Yuta. Wall following using angle information measured by a single ultrasonic transducer. In *Proceedings of the 1998 IEEE International Conference on Robotics and Automation*, pages 1590–1596, May 1998.

[102] R Zapata, P Lepinay, and P Thompson. Reactive behaviors of fast mobile robots. *Journal of Robotic Systems*, 11(1):13–20, 1994.